Corrosion Science 240 (2024) 112485

Contents lists available at ScienceDirect

Corrosion Science

journal homepage: www.elsevier.com/locate/corsci

Synergistic effects of Pt and Y addition in (Ni, Pt)CrAlY bond coat on oxide spallation resistance and growth of interdiffusion zone between bond coat and Ni-based single crystal superalloy

Ujjval Bansal [a,b,*], Neelamegan Esakkiraja [a,c], Thangaraj Baskaran [a], Tanaji Paul [a,d], Raju Ravi [a], Praveen Kumar [a], Vikram Jayaram [a], Aloke Paul [a,**]

[a] Department of Materials Engineering, Indian Institute of Science, Bengaluru 560012, India
[b] Institute for Applied Materials, Karlsruhe Institute of Technology, Karlsruhe 76131, Germany
[c] Institute of Materials Physics, University of Münster, Wilhelm-Klemm-Str. 10, Münster 48149, Germany
[d] Department of Mechanical & Materials Engineering, Florida International University, 10555 West Flagler St, Miami, FL, USA

ARTICLE INFO

Keywords:
Diffusion
Oxidation
Microstructure
Bond coat
Superalloy

ABSTRACT

This study shows the beneficial effect of Pt addition to the (β+γ)-NiCrAlY coating. Adding Y in NiCrAl increases oxide growth kinetics but improves spallation resistance. Pt with Y does not change the oxidation rate compared to only adding Y but significantly reduces spallation when cooled to room temperature. Continuous layers of Al_2O_3 and Cr_2O_3, along with other oxides such as $YAlO_3$, $NiCr_2O_4$, and $NiAl_2O_4$, are observed. Moreover, Pt addition reduces the thickness of the interdiffusion zone where Al goes through an uphill diffusion profile, minimizing Al loss and significantly decreasing the growth of deleterious TCP phases.

1. Introduction

Ni-based superalloys are coated with MCrAlY (where M = Ni or Ni and Co) overlay or β-Ni(Pt)Al diffusion coatings in turbine blades for oxidation protection of the superalloy substrate due to their propensity to generate a protective oxide layer when exposed to elevated temperatures [1–9]. These coating layers act as the Al reservoir for the continuous growth of Al_2O_3. The oxide layer also helps create a bond between the metallic (or intermetallic) bond coat and yttria-stabilized zirconia (YSZ) for thermal protection. The oxygen diffusion rate through the α-Al_2O_3 is very low. This ensures a slow rate of scale growth, minimizing the deleterious effects of residual stress for better spallation resistance and compositional changes, thereby extending the lifetime of the coating. The Pt-modified diffusion coating offers an effective solution for augmenting the adhesion of oxide scales [6,7]. It is suggested that adding Pt reduces the sulphur segregation at the bond-coat Al_2O_3 oxide interface, improving the adhesion strength, i.e., the spallation resistance [10–16]. On the other hand, a recent study on thermal cycle tests of β-Ni(Pt)Al alloy indicated the improvement of spallation resistance in air, i.e. in the absence of sulphur segregation [12,15,17,18]. This suggests an improvement in adhesion strength and a reduction in the growth of the Kirkendall voids, possibly because of changes in the diffusion rates of elements [19,20]. However, a significant disadvantage of Pt addition to β-Ni(Pt)Al is the increased growth of the topological closed-packed (TCP) precipitate-containing interdiffusion zone between the superalloy and the bond coat. Pt addition increases the interdiffusion rates of Ni and Al in the β-NiAl phase by increasing the concentration of the defects (vacancies and antisites) and decreasing the migration energy [19–22]. This is a severe issue since the brittle precipitate-containing zone is one of the weakest zones of the superalloy coating system and is prone to developing cracks. Moreover, the unwanted consumption of Al for the growth of the interdiffusion zone is much higher than the use of Al for the growth of the Al_2O_3 oxide layer. This has led to further research for an alternate material that can reduce the interdiffusion zone's growth without losing the oxide layer's thermal cycling resistance when it replaces Pt partially or completely for the β-Ni(Pt)Al diffusion coating [17].

The use of Y in MCrAl overlay coating is followed by the known positive effects in FeCrAl alloys, in which yttrium significantly improved performance [23–25]. This has been shown to improve oxide scale adherence by facilitating the formation of oxide pegs at the oxide/bond-coat interface. When Y concentration is increased,

* Corresponding author at: Institute for Applied Materials, Karlsruhe Institute of Technology, Karlsruhe 76131, Germany.
** Corresponding author.
E-mail addresses: ujjval.bansal@kit.edu (U. Bansal), aloke@iisc.ac.in (A. Paul).

https://doi.org/10.1016/j.corsci.2024.112485
Received 19 June 2024; Received in revised form 28 August 2024; Accepted 25 September 2024
Available online 27 September 2024
0010-938X/© 2024 The Author(s). Published by Elsevier Ltd. This is an open access article under the CC BY-NC license (http://creativecommons.org/licenses/by-nc/4.0/).

segregation at oxide grain boundaries occurs, impacting species diffusion and ultimately influencing the rate of oxide scales [25]. A further improvement in the spallation resistance of the oxide layer, especially at higher temperature ranges, is a subject of intense research by alloying additions such as Ta, Hf, Si, Re, Pt, etc. [26–32]. In general, Ta, Hf, Si, and Re are added to the alloy, whereas the use of Pt is practiced differently. The oxidation resistance is improved when Pt is electroplated after depositing the MCrAlY coating and diffusion annealed. Pt is sometimes electroplated before and after the MCrAlY deposition to report improved overall coating properties [33,34]. Sometimes, Pt powder is ball-milled with MCrAlY powder to develop an alloy [35]. However, the complete effect of Pt addition may not be evident unless annealed for enough time. Moreover, a comprehensive study is still missing delineating the role of Y and Pt in improving performance. An in-depth analysis is required to understand the role of these elements on the stability and growth characteristics of the oxide layer and whether the addition of Pt increases or decreases the growth of the unwanted precipitate-containing interdiffusion zone by consumption of Al from the bond coat.

In this paper, we present a systematic study on NiCrAl bond coat alloys modified with Pt and Y, individually and jointly, to report a significant increase in spallation resistance in the presence of both elements. The oxidation experiments were conducted in air at 1100 °C for varying durations to comprehensively explore the oxide scale's growth characteristics and microstructural evolution. This highlights the underlying mechanisms for enhanced oxidation resistance when employing Pt and Y modifications. Further, we report a significant decrease in the volume fraction of brittle TCP phases because of Pt addition. These indicate the benefits of the addition of Pt addition on both, i.e. oxide spallation resistance and growth of unwanted TCP phases, in contrast to the effect of Pt addition in β-NiAl diffusion coating in which it enhances the spallation resistance of the oxide layer but increases the volume fraction of TCP phases in the interdiffusion zone. The role of Pt addition to both types of coating alloys is compared in detail considering the diffusion rates of elements. These findings contribute to our understanding of improved protective coatings and offer valuable insights for developing advanced solutions tailored to meet the demands of challenging applications at elevated temperatures.

2. Materials and methods

The bond-coat alloys with nominal compositions (at%), as outlined in Table 1, were vacuum arc melted under an argon atmosphere. All the metals utilized were high purity (99.99 %) and sourced from Alfa Aesar. The melt buttons were flipped 7–8 times to avoid macro segregations and ensure chemical homogeneity. Subsequently, the melt buttons were homogenized at 1200 °C for 100 h in a high vacuum (~10^{-4} Pa) furnace. After homogenization, the alloy composition was quantified using an electron probe micro-analyzer (EPMA, JXA-8530F) equipped with a wavelength dispersive spectroscopy (WDS).

Samples of dimensions 7 mm × 5 mm × 1.5 mm were sectioned using an electro-discharge machine (EDM) for microstructural investigation and oxidation studies. These samples were subsequently polished to a mirror finish for microstructural characterization. The microstructural examination was conducted using a scanning electron microscope (SEM, FEI SEM Quanta 200) with a W source. The composition of individual phases was determined using EPMA, as listed in Table 1.

For the oxidation studies, the samples were annealed in a box furnace at 1100 °C (±5 °C) for 100, 250 and 500 h in air. After annealing, the samples were cooled in an open atmosphere by placing them at room temperature. The X-ray diffractometer (X-pert PRO, PANalytical) with monochromatic Cu-Kα radiation was used for the phase analysis of the oxide samples. Cross-section samples were prepared by cutting the samples using a slow-speed diamond saw (IsoMet™ low-speed precision cutter, Buehler, USA), followed by grinding and polishing for SEM analysis. The microstructure of the top surface and the cross-section were characterized using SEM.

A commercial CMSX-4 superalloy was used to prepare superalloy/bond-coat diffusion couples. The average composition of superalloy is detailed in Table 2. Samples from superalloy and bond-coat alloys were sectioned using a slow-speed diamond blade followed by metallographic polishing to obtain flat and smooth surfaces. The samples were then joined using a special fixture for producing diffusion couples and then annealed at 1100 °C (±5 °C) for 64 h in a high vacuum furnace (10^{-4} Pa). Post-diffusion annealing, the couples were cross-sectioned and polished for microstructural analysis. Focused ion beam milling in a dual-beam SEM (FIB-SEM, SCIOS) was used to lift electron transparent lamella from the inter-diffusion zone (IDZ). Precipitates and phases within IDZ were examined in a transmission electron microscope (TEM) (ThermoFisher® TecnaiTM T20) equipped with a LaB_6 filament operated at 200 kV. The composition analysis was carried out by elemental mapping using energy-dispersive spectroscopy (EDS) using a Super-X detector equipped in a TEM (ThermoFisher® Titan™ Themis) operating at 300 kV.

3. Results

3.1. Microstructure of the bond-coat alloys

Fig. 1 shows the BSE micrographs of bond coat alloys after homogenization. The resulting microstructure consists of β and γ phases. Pt-containing alloys exhibit an inverted contrast of β phase compared to the Pt-free bond coats. The compositions of β and γ phases in all bond coat alloys are provided in Table 1. While Ni content is similar in both phases, Al content is higher in the β- and Cr content is higher in the γ-phase. Pt partitions with higher concentration in β- than the γ-phase in the Pt-containing alloys. The fractions of β- and γ- phases are almost equal in the absence of Pt. With the addition of Pt, the fraction of the β-phase decreases and the fraction of the γ-phase increases by 5 ± 2 %. In the Pt-free alloys, the higher Cr: Al ratio governs the brighter contrast for the γ-phase compared to the β-phase. The higher Pt content within the β-phase gives rise to a pronounced bright contrast in Pt-containing bond-coat alloys compared to the relatively dark contrast for the γ-phase. WDS analysis indicates that adding Y forms a Ni_5Y-based intermetallic compound. The accurate composition of this compound is difficult to measure by EPMA because of its small size. However, the ratio of Ni and Y is close to this compound's composition. Some other elements may also be present in small quantities. Earlier reports also

Table 1
Composition (at%) of bond coat alloys and different phases measured from EPMA. The average composition and the error range are calculated from at least 10 WDS point analyses.

Nominal composition (Designations)		Actual composition in different phases (at%)							
		β				γ			
		Pt	Ni	Cr	Al	Pt	Ni	Cr	Al
Yttrium-free	$Ni_{59.3}Cr_{21.7}Al_{19}$ (NiCrAl)	-	59.5 ± 0.2	12.0 ± 0.2	28.8 ± 0.1	-	58.8 ± 0.2	29.4 ± 0.2	11.8 ± 0.2
	$Ni_{49.3}Pt_{10}Cr_{21.7}Al_{19}$ (NiPtCrAl)	12.4 ± 0.2	47.1 ± 0.3	12.1 ± 0.2	28.4 ± 0.2	8.5 ± 0.1	51.0 ± 0.2	28.2 ± 0.2	12.4 ± 0.1
Yttrium-containing	$Ni_{59}Cr_{21.7}Al_{19}$ (NiCrAlY)	-	59.5 ± 0.3	12.2 ± 0.3	28.2 ± 0.1	-	58.4 ± 0.2	30.2 ± 0.1	11.4 ± 0.2
	$Ni_{49}Pt_{10}Cr_{21.7}Al_{19}$ (NiPtCrAlY)	12.0 ± 0.2	47.3 ± 0.2	11.4 ± 0.6	29.4 ± 0.6	8.0 ± 0.2	50.9 ± 0.2	29.3 ± 0.3	11.7 ± 0.2

Table 2
Composition (at%) of CMSX-4 superalloy and elemental partitioning in γ and γ' phases. The partitioning of elements in different phases in comparison to reported values in Ref. [36].

Element (at%)	Co	Cr	Al	Ti	Ta	Mo	W	Re	Ni
CMSX 4	9.0 ± 1.6	7.0 ± 1.2	12.3 ± 1.8	1.5 ± 0.3	2.1 ± 0.4	0.3 ± 0.2	1.7 ± 0.2	1.0 ± 0.3	65.7 ± 2.1
γ	13.0	16.9	4.5	0.2	0.5	-*	2.5	2.2	60.2
γ'	5.6	2.5	16.6	1.9	3.0	-*	1.2	0.3	68.9

-*: uncertain

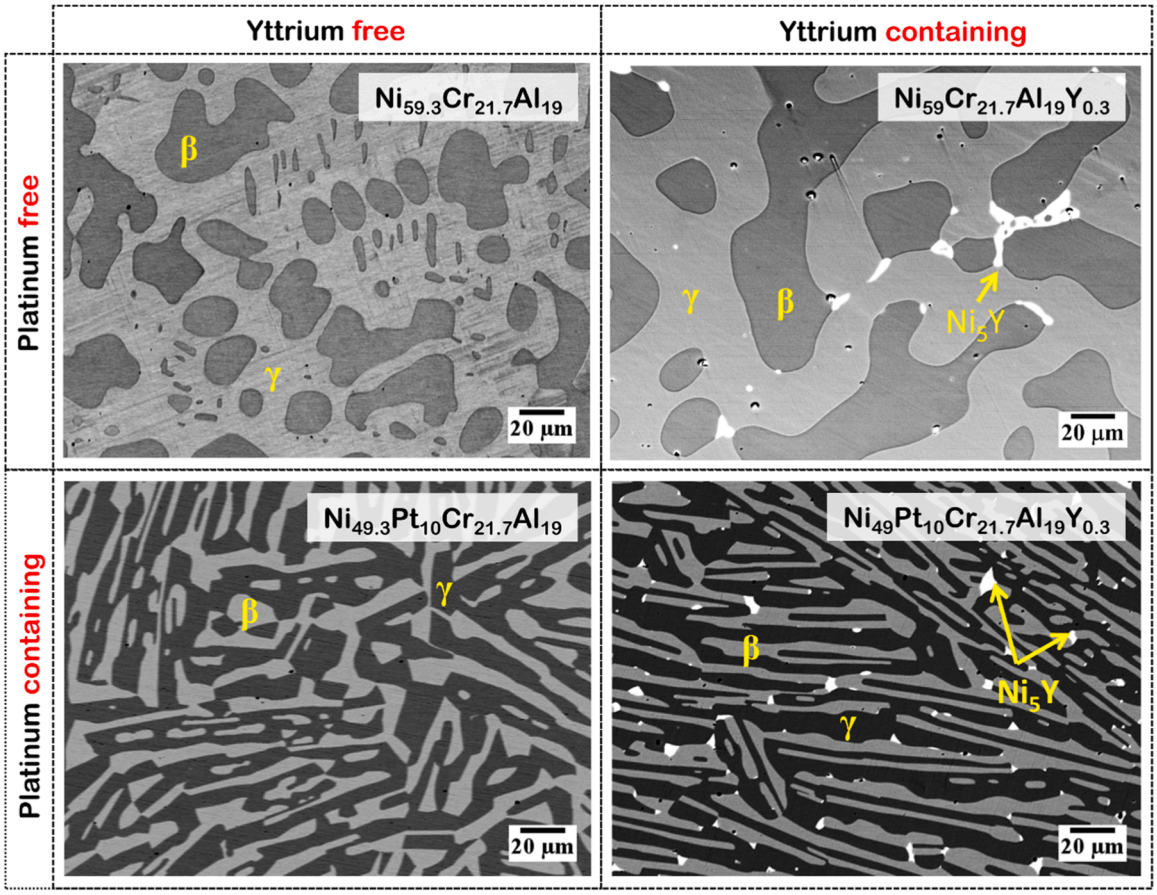

Fig. 1. : Backscattered electron (BSE) micrographs of (a) $Ni_{59.3}Cr_{21.7}Al_{19}$, (b) $Ni_{59}Cr_{21.7}Al_{19}Y_{0.3}$, (c) $Ni_{49.3}Pt_{10}Cr_{21.7}Al_{19}$, and (d) $Ni_{49.3}Pt_{10}Cr_{21.7}Al_{19}Y_{0.3}$ bond coat alloys after homogenization at 1200 °C for 100 h. Evident in the micrographs are both β and γ phases. The Ni_5Y appears as the bright phase.

indicate the formation of the Ni_5Y phase in bond-coat alloys with similar compositions, such as Ni-20Co-19Cr-24Al-0.2Y alloys [37–39]. Further, the partitioning of Y to β- and γ-phase is limited (<0.02 %; therefore, not detected by WDS) due to the immiscibility of Y in these phases. Consequently, Y is confined as the Ni_5Y phase at the β/γ phase boundary, as highlighted in Fig. 1. The fraction of this phase, measured using Image processing techniques with Python, is found to be 1.9 ± 0.3 and 1.6 ± 0.2 %, respectively, for NiCrAlY and NiPtCrAlY bond-coat alloys.

3.2. Post-oxidation microstructural analysis

The Pt-free or Pt-modified β-NiAl diffusion coatings are known to grow the α-Al_2O_3 oxide layer [17,40–43]. Adding Pt improves spallation resistance without sulphur segregation [10,15,41]. On the other hand, MCrAlY is known to grow mixed oxide layers [8]. The difference in adherence and spallation of the oxide layers after isothermal annealing at 1100 °C at different intervals are shown in Fig. 2. The oxide layer, which remained adhered to the bond-coat alloy after cooling to the room temperature in air, appears dark in the microstructure compared to the substrate with brighter contrast because of spallation.Fig. 3 displays the bar graph of measured area fractions of the oxide layer after air cooling to room temperature from 1100 °C for all bond coat alloys oxidized for 100, 250 and 500 h. Images from 3 to 5 different regions were used for the data in Fig. 3. Image processing technique with Python was employed to count pixels corresponding to the un-spalled (oxide layer) and spalled (substrate) region. First, the image was converted to gray-scale, and then, the threshold was used to create a binary image segmenting different phases, in the present case, the substrate and oxide layer. The area fractions were then determined by counting the pixels corresponding to each phase and calculating their proportions relative to the total number of pixels. This process accurately estimated the un-spalled oxide layer and substrate (spalled region). Interestingly, adding Y to NiCrAl improved adherence marginally at this temperature of isothermal oxidation and air cooling. Pt addition to the same alloy is shown to have better adherence. On the other hand, in the presence of both Y and Pt, the spallation resistance improved significantly. The oxide did not show any spallation due to air cooling after 100 h of oxidation. It spalled a little after 250 h and showed higher spalling after 500 h isothermal oxidation. To investigate further, the cross-section of the microstructure of bond-coat alloys and the average thickness of the

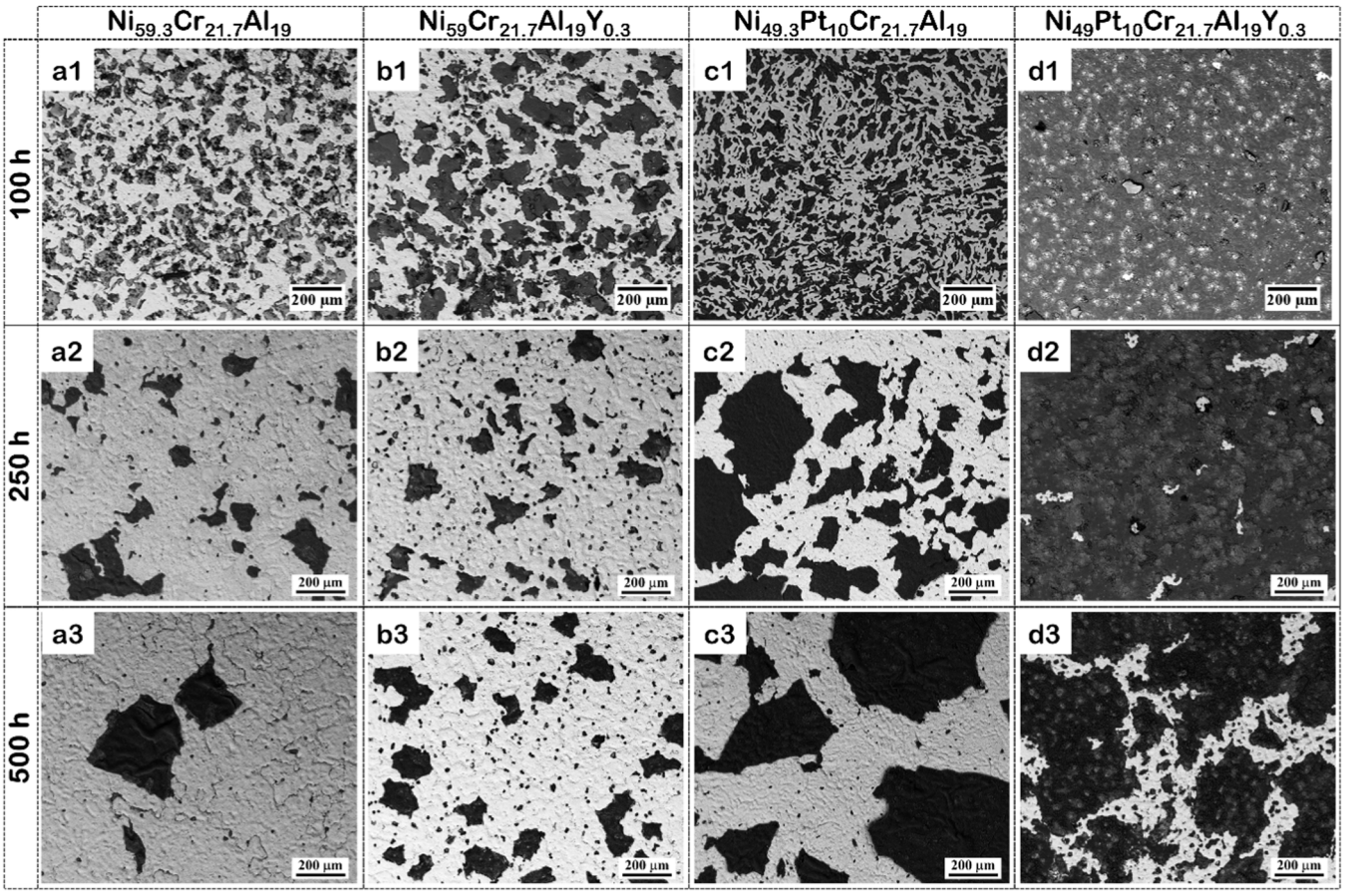

Fig. 2. : Backscattered electron (BSE) micrographs of the top surface of (a1–3) $Ni_{59.3}Cr_{21.7}Al_{19}$, (b1–3) $Ni_{59}Cr_{21.7}Al_{19}Y_{0.3}$, (c1–3) $Ni_{49.3}Pt_{10}Cr_{21.7}Al_{19}$, and (d1–3) $Ni_{49}Pt_{10}Cr_{21.7}Al_{19}Y_{0.3}$ bond coat alloys after isothermal oxidation at 1100 °C for 100, 250 and 500 h. Notably, the dark regions on the micrographs indicate the presence of adherent oxide layers on the surface.

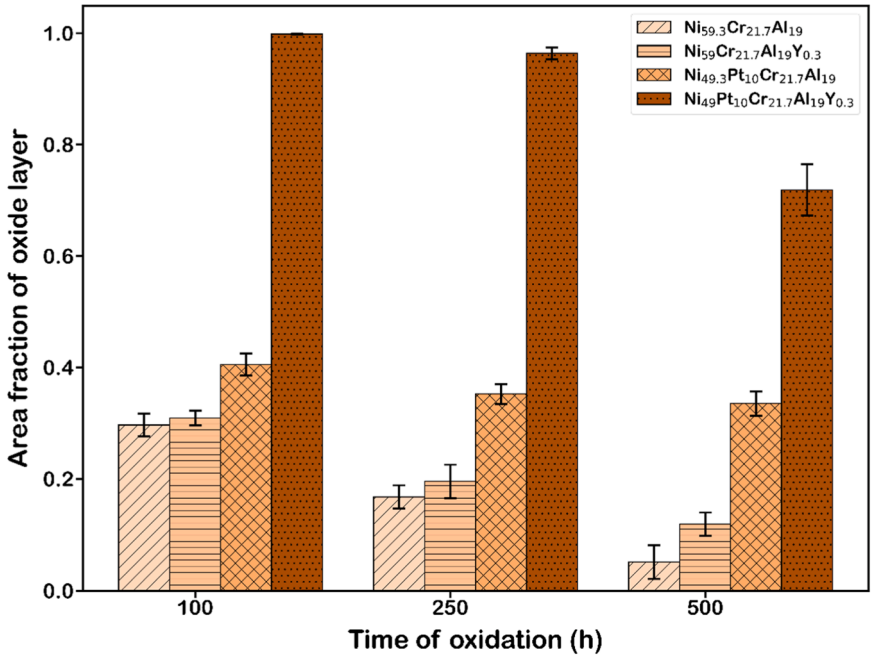

Fig. 3. : Plot of the area fraction of oxide layer adhered to all the bond-coat alloys upon cooling to the room temperature after isothermal oxidation for 100, 250 and 500 h at 1100 °C.

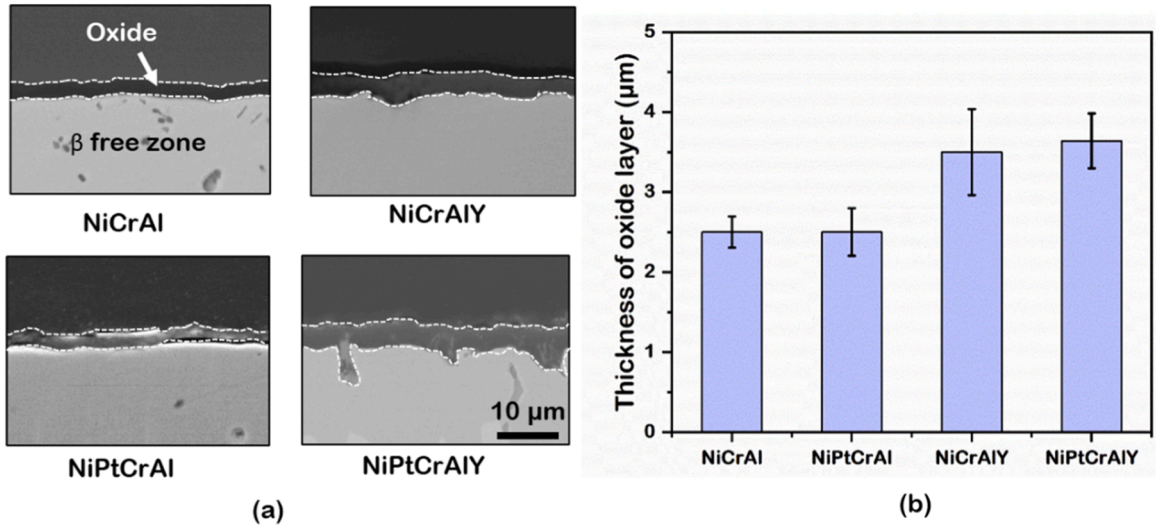

Fig. 4. : Bond coat alloys after oxidation for 100 h at 1100 °C. (a) Cross-sectional micrograph showing the oxide layer (from the un-spalled region) and β-free zone, and (b) Plot of oxide layer thickness.

oxide layers are shown after oxidation for 100 h in Fig. 4. Images from at least three regions were utilized in ImageJ software to estimate thickness. It's worth emphasizing that the oxide layer cross-section microstructures were examined from the un-spalled oxide layer to understand the growth mechanism. It can be seen that the addition of Y increases the thickness of the oxide layer, although the addition of Pt did not increase it. Adding Pt and Y together resulted in an almost similar thickness of the oxide scale compared to the oxide thickness when only Y was added. These indicate the improvement of adhesion due to the coexistence of these elements, although Pt has a more significant influence.

The higher fraction of adhered oxide layer for Ni(Pt)CrAlY bond coat, even after 500 h, facilitates the examination of the microstructural evolution of the substrate adjacent to the oxide layer as a function of time, as shown in Fig. 5. In this coating, β-NiAl acts as the Al reservoir, and γ-NiAl solid solution provides the necessary strength for the property balance. When Al is consumed to grow the Al_2O_3 oxide, the β-phase is converted to the γ phase. Therefore, only the γ phase is found adjacent to the oxide layer. With increasing annealing time and thickness of the oxide layer, the length of the γ-phase adjacent to the oxide layer also increases, which is evident in Fig. 5.

The BSE image shown in Fig. 5 indicates the presence of possibly two distinctive continuous oxide phase layers as separated by a dashed line. The quantitative map analysis by EPMA indicates the different types of oxides present. As shown in Fig. 6 from the 250 h oxidized sample, WDS mapping illustrates that the oxide layer next to the bond coat alloy is rich in Al (α-Al_2O_3) followed by a top layer of Cr-rich (Cr_2O_3). Further, Y-Al-rich oxide particles ($YAlO_3$) are found at the substrate/oxide interface, inside the Al-rich oxide layer, and also extended internally in the

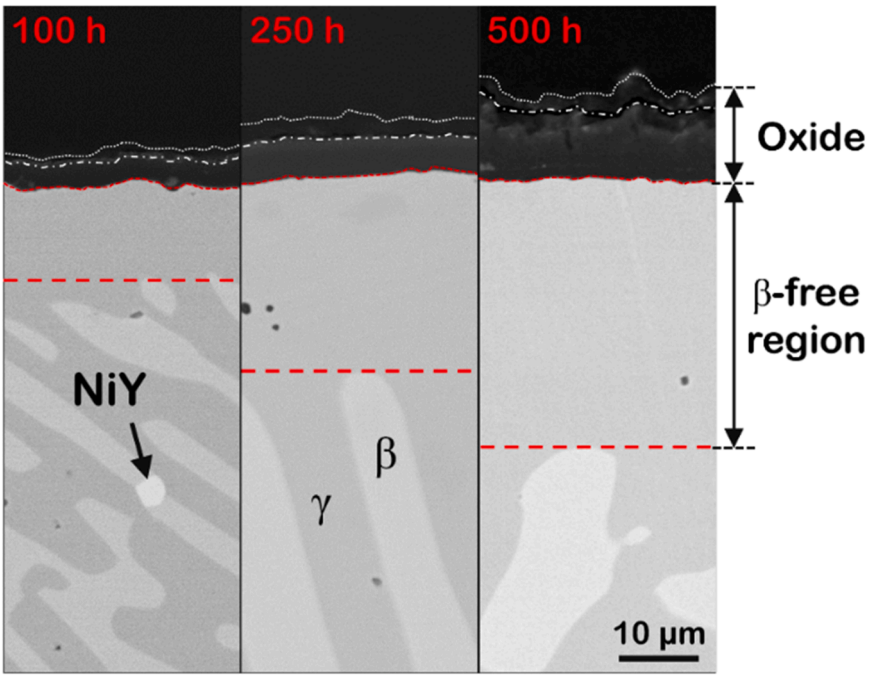

Fig. 5. : Cross-sectional micrograph of $Ni_{49}Pt_{10}Cr_{21.7}Al_{19}Y_{0.3}$ bond coat alloy following oxidation for 100, 250, and 500 h at 1100 °C. The images reveal the progressive development of the oxide layer over time and the corresponding expansion of the β-free region. Note that the voids were not found at the oxide-bond coat interface.

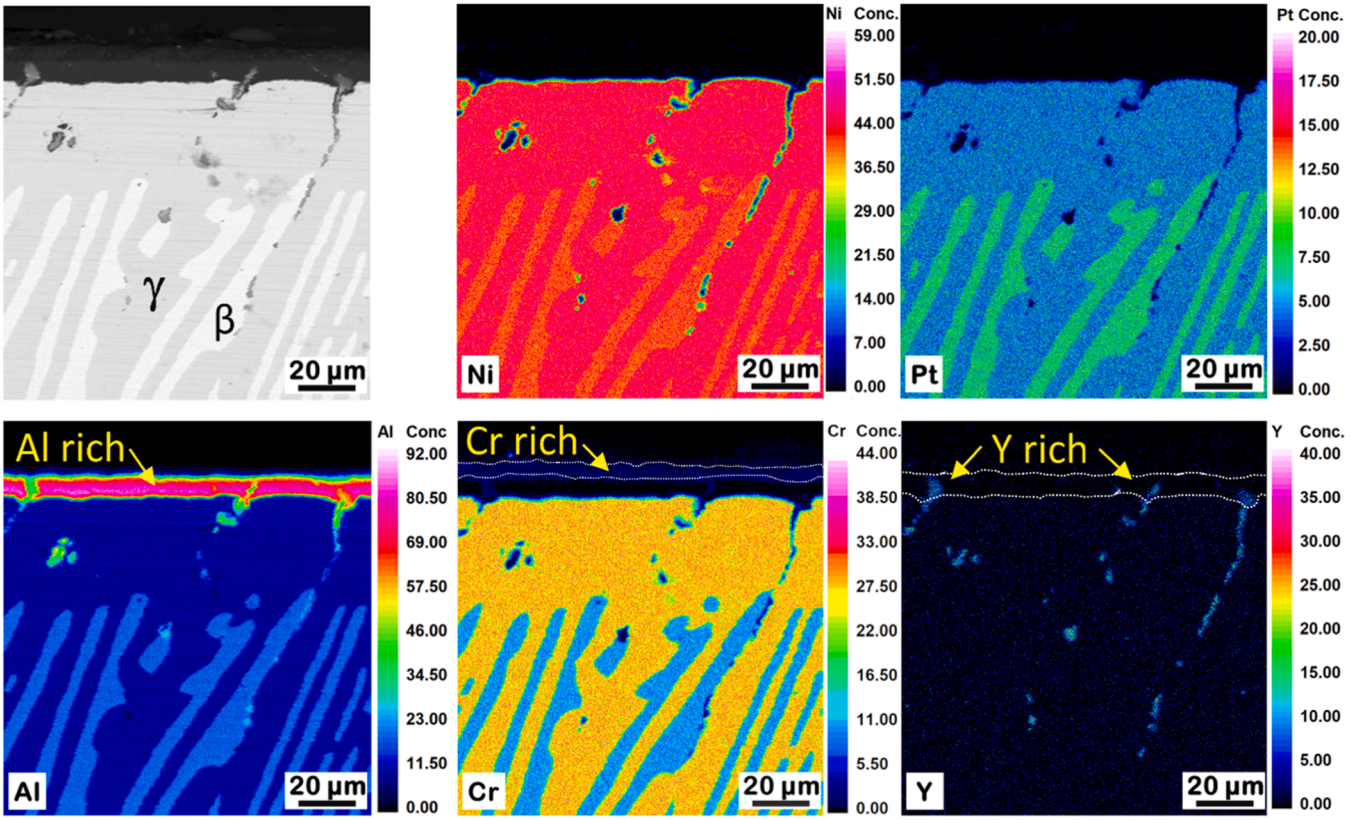

Fig. 6. : Cross-sectional wavelength-dispersive spectroscopy (WDS) mapping revealing the compositional distribution in the oxide layer adjacent to the oxidized $Ni_{49}Pt_{10}Cr_{21.7}Al_{19}Y_{0.3}$ bond coat alloy for 250 h at 1100 °C. The layer exhibits a distinct Al-rich region (α-Al_2O_3), succeeded by a Cr-rich layer (Cr_2O_3). Notably, the Al and Y containing oxide particles are found in the substrate-oxide interface and also inside the substrate.

adjacent γ- and the two-phase (β+γ) region. These could be detected as Y-Al-rich oxides instead of Ni_5Y intermetallic compounds by the presence of Al (TEM analysis as discussed next). The Y-Al-rich oxides can grow inside the substrate because of oxygen availability. It is known that oxygen solubility is higher in the γ- compared to the β-phase [44,45]. Oxide particles are found at the γ/β phase boundaries when the original Ni_5Y intermetallic compound converts to Y-Al-containing oxide. The presence of these oxides in the γ-phase adjacent to the oxide layer indicates the original γ/β interface locations, which ultimately convert to the γ-phase with the loss of Al from the β-phase.

Fig. 7 displays a high-resolution SEM image of the oxide layer on the NiPtCrAlY bond-coat alloy following a 250-hour oxidation period. The micrograph notably highlights a duplex grain morphology, a common characteristic observed in α-Al_2O_3 oxide layers in bond-coat alloys, even on the β-Ni(Pt)Al diffusion coating [17]. The long columnar grains are grown from the bond coat/oxide interface (interface I) because of the diffusion of oxygen through the phase layer. On the other hand, the same phase grows differently from the α-Al_2O_3/Cr_2O_3 interface (interface II) with relatively smaller grains. The plane demarcating these distinct grain morphologies corresponds to the Kirkendall marker plane position [46]. Cr_2O_3 oxide layer with a much smaller thickness grows between interface II and III, *i.e.* between the α-Al_2O_3 and air at the temperature of oxidation (1100 °C). Moreover, $NiAl_2O_4$ spinel also grows on the top, which could not be retained for cross-sectional analysis in the electron microscope because of its fragile nature.

The probe size of EPMA does not allow the identification of any other types of oxides from the composition map (Fig. 6), which may be present as small particles. Therefore, X-ray diffraction (XRD) analysis of the top surface of NiPtCrAlY bond coat alloys after oxidation for 500 h was conducted to identify the different types of oxides present in the oxide layer. Fig. 8 shows the indexed XRD pattern for NiPtCrAlY alloys. The strong peak observed corresponds to the α-Al_2O_3, indexed according to the standard diffraction file PCPDF #03–065–0420. No peaks corresponding to the other variants of Al_2O_3 oxides were observed, suggesting the complete transformation to a stable α-Al_2O_3 variant. Other variants of the alumina, which may grow at the initial stage of oxidation on the β-phase, are reported to transform into the most stable α-Al_2O_3 with increasing oxidation time [42,43,47–53], which subsequently converts to spinel [54]. We have observed peaks corresponding to spinels, although it is very difficult to differentiate since peaks from different spinels overlap. The presence of the Cr_2O_3 (outer Cr-rich layer, as indicated in Fig. 7), is also confirmed and indexed according to the standard diffraction file JCPDS #038–1479. No peaks corresponding to Y and Al-rich intermetallic compounds are observed in XRD, possibly due to the very low volume fraction of such phases.

The X-ray diffraction analysis indicates a possibility of finding mixed oxides. Using FIB techniques, an electron transparent lamella for the TEM studies was prepared from the NiPtCrAlY bond-coat alloy and oxides interface. A bright field TEM image of different oxides is shown in Fig. 9(a1-d1), highlighting their morphologies. The selected area diffraction pattern (SADP) from the coarse columnar grain of the oxide layer adjacent to the bond-coat alloy is shown in Fig. 9(a). It is indexed as a hexagonal oxide, α-Al_2O_3, with space group R-3c. Further, the phase presented in Fig. 9(b) exhibits a notable enrichment of Y and Al, a feature substantiated by the qualitative EDS maps provided in Fig. 10. The SADP from these Y-Al-rich oxides corresponds to an orthorhombic crystal structure, with Pnma space group conclusively identified as $YAlO_3$ oxide. The oxide in pegs was also identified as $YAlO_3$. Oxide pegging has been reported to improve the oxide-scale adherence in a system like FeCrAlY [23,25], CoCrAlY [55] and CoAlWY superalloys [56]. The outer layer, as expected, is indexed as hexagonal Cr_2O_3 oxide with a space group R-3c, as shown in Fig. 9(c). Moreover, the diffraction

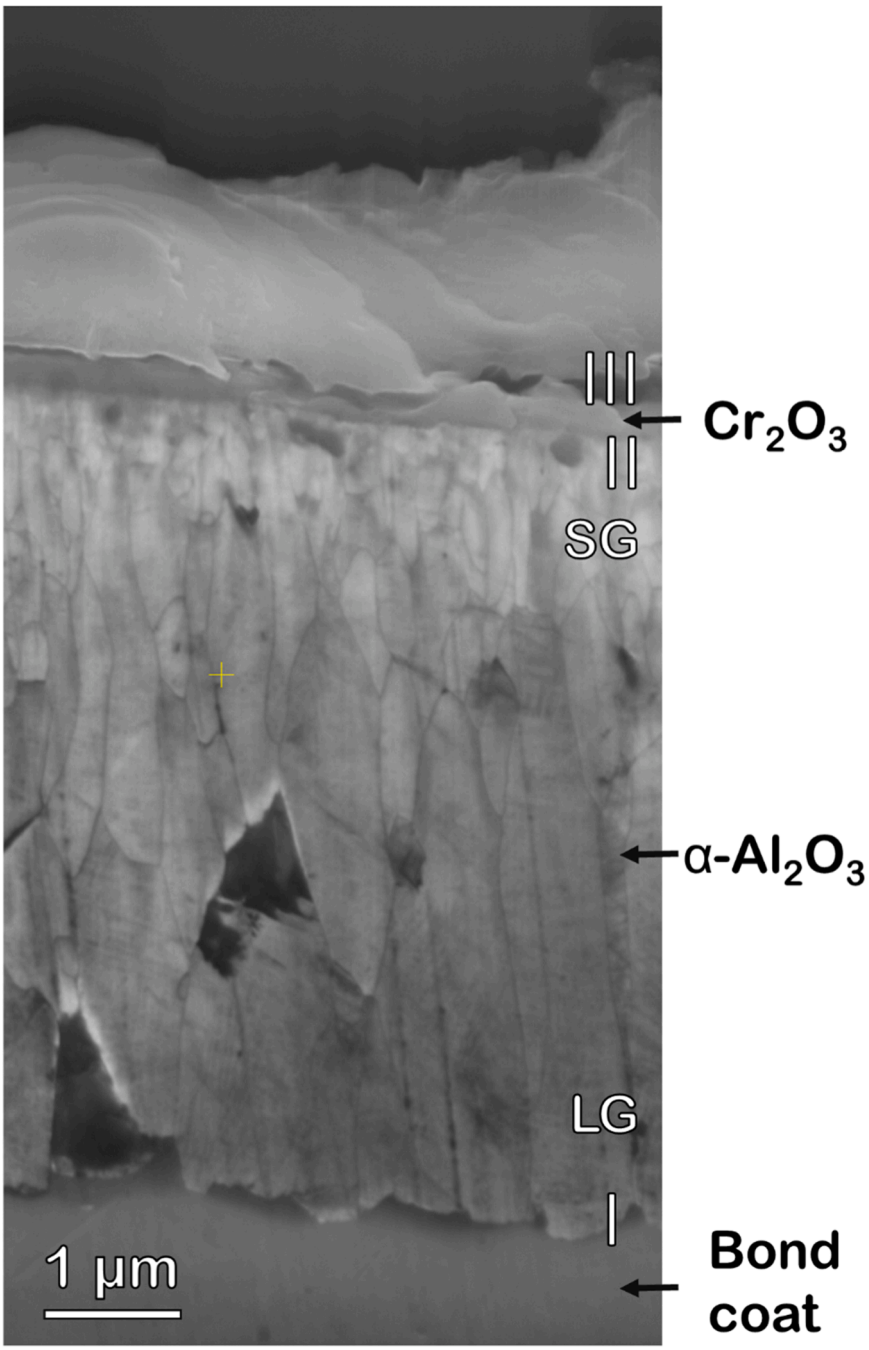

Fig. 7. : Cross-sectional SEM micrograph of the oxide on $Ni_{49}Pt_{10}Cr_{21.7}Al_{19}Y_{0.3}$ bond coat at high magnification showing the bond-coat alloy at the bottom, followed by the duplex grain morphology in α-Al_2O_3 oxide layer (LG: long grains and SG: short grains) and Cr_2O_3 layer at the top. I, II, and III mark different interfaces. The oxide surface on the top side is exposed due to a visible tilt angle of 2.5° during imaging.

pattern also confirms the presence of the cubic $NiCr_2O_4$ spinel oxide particles (space group: Fd-3m) embedded mostly in the Al_2O_3 layer, as shown in Fig. 9(d).

Interesting surface topological features after oxidation are found, as shown in Fig. 11. At the initial stage, oxides grow from both β- and γ-phases of the bond coat differently. It is already known that α-Al_2O_3 grows with a ridge structure on the β-NiPtAl phase [17]. A similar morphology is also found on the oxide surface above the β-phase in this NiCrAlPtY bond coat. The oxide layer on the γ-phase does not show a ridge-type structure, resulting in a relatively smooth surface. The difference in the growth of oxides above the β- and γ- phases is also reported earlier [8]. Only Al_2O_3 is found to be favorable to grow on the β-phase. Initially, transient oxide θ-Al_2O_3 with needle-type structure may grow, but it later converts to more stable α-Al_2O_3 and subsequently converts to spinel, as discussed later. Growth of both these oxides (θ- and α-Al_2O_3) is reported at the early stage of oxidation [8,49]. The oxide layer grows differently on the γ-phase. Al_2O_3, Cr_2O_3 and Spinel are reported to grow on the γ-phase from the beginning [8]. As shown in Fig. 5, the β-phase of Ni(Pt)CrAlY converts to the γ-phase with the loss of Al because of oxidation. Therefore, the oxide layer grows on the γ-phase after the initial stage with increasing annealing time [8]. Thus, such a characteristic surface morphology indicates that oxides grew from two different phases at the early stages of oxidation differently. Because of surface roughness, accurate composition analysis is not possible. However, EPMA analysis indicated the presence of high concentrations of Ni and Al, identifying these as $NiAl_2O_4$ spinel (see Fig. S1 in supplementary

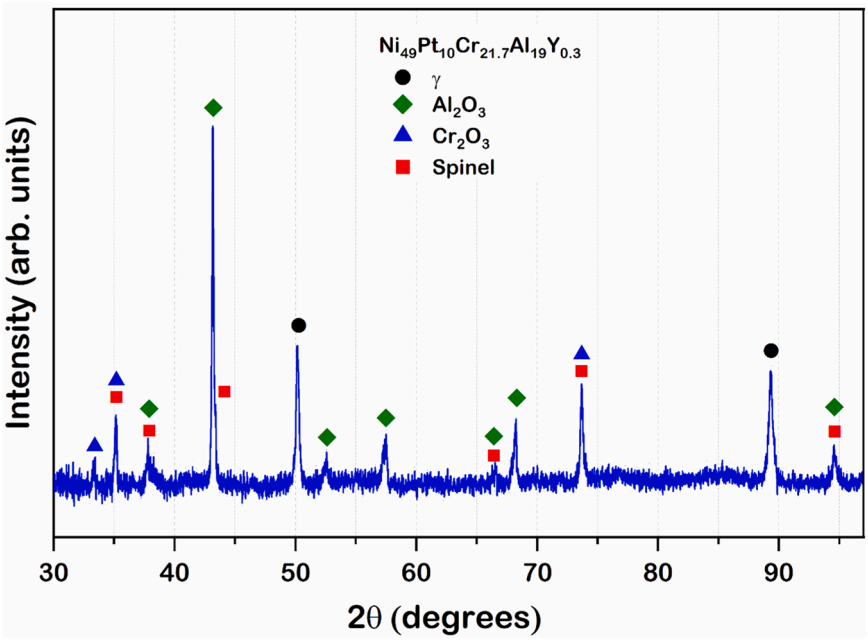

Fig. 8. : X-ray diffraction analysis of oxidized $Ni_{49}Pt_{10}Cr_{21.7}Al_{19}Y_{0.3}$ bond coat alloys for 500 h.

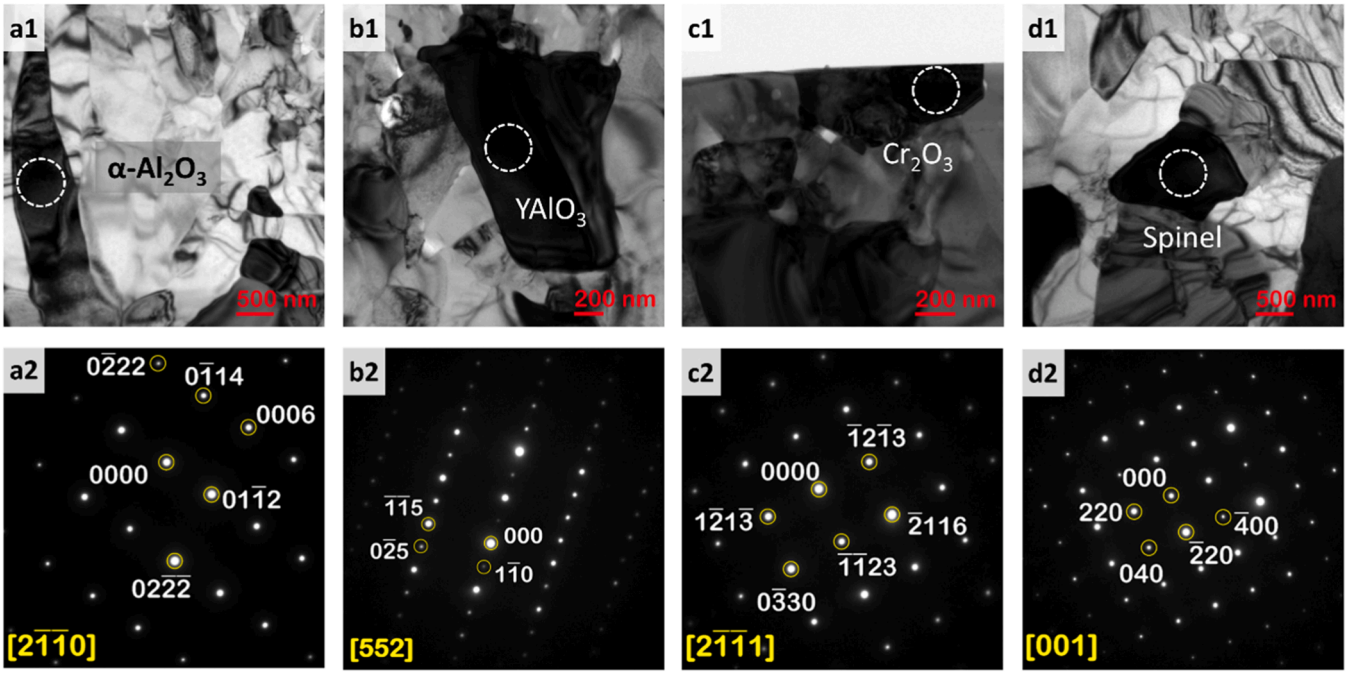

Fig. 9. : TEM analysis of the oxide layer, featuring bright field micrographs paired with corresponding diffraction patterns. (a1, a2) α-Al_2O_3, (b1, b2) $YAlO_3$, (c1, c2) Cr_2O_3, and (d) spinel.

file). At certain locations, even Cr with a bit higher concentration was also found, which indicates the growth of $Ni(Al,Cr)_2O_4$ spinel as well. The presence of these oxides is reported in several published articles [50–53,57–60]. Therefore, the Al_2O_3, which grew with a ridge structure, was subsequently converted to spinel by reacting with NiO and Cr_2O_3 without losing the shape completely [50]. The needle-like oxides could be the sign of the initial growth of θ-Al_2O_3 [8,47,48,54], which later converted to spinel as well without losing its shape [54]. The growth mechanism is explained in detail in Section 4.

3.3. Growth of interdiffusion zone (IDZ) between Ni(Pt)CrAl bond coats and CMSX-4 Superalloy

Growth of the interdiffusion zone (IDZ) between the bond coat and superalloy is an essential aspect of the study because of the unwanted loss of Al from the bond coat for the growth of this part. The unwanted loss of Al for the growth of this IDZ is much higher than the Al used for the growth of the oxide phase, which protects the substrate [17]. Moreover, the growth of the brittle TCP phases is an issue that is caused by the rejection of alloying elements, such as Re, W, Ta, etc., from the matrix with the loss of Ni from the Ni-rich superalloy and increase in Al

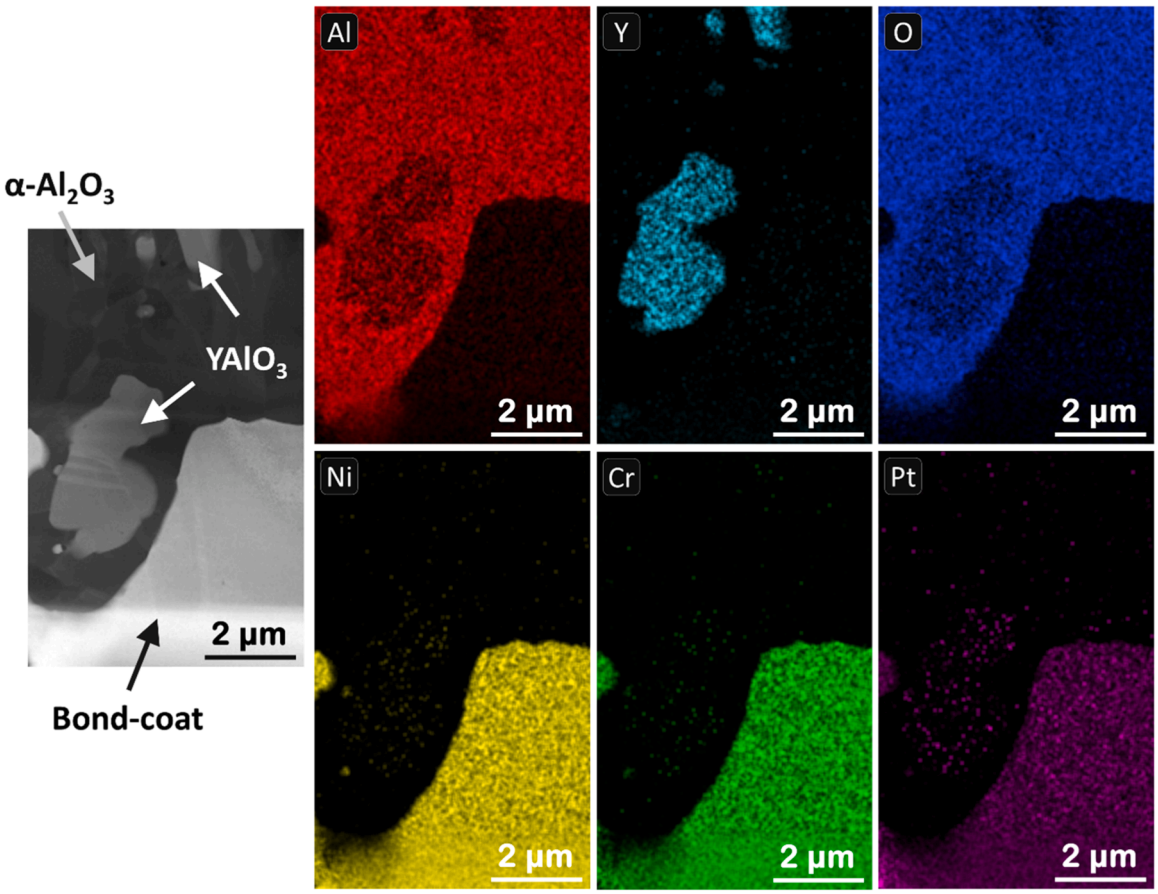

Fig. 10. : STEM-EDS maps of all elements indicate the Y-rich $YAlO_3$ oxide in the protrusions at the bond-coat/oxide interface and the α-Al_2O_3 layer.

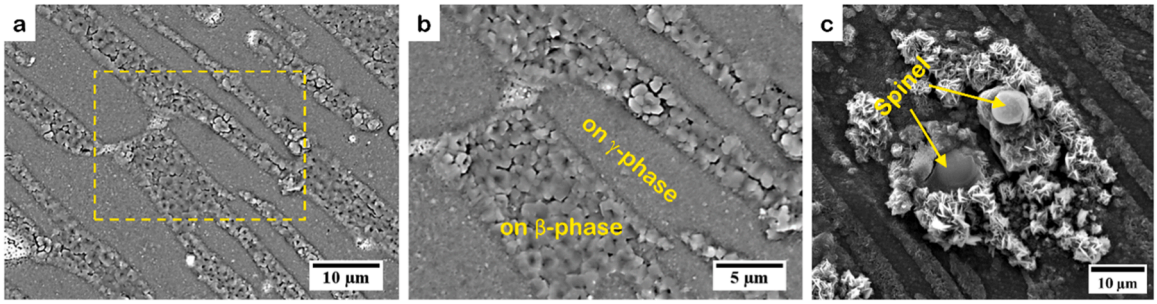

Fig. 11. : Surface morphology of $Ni_{49}Pt_{10}Cr_{21.7}Al_{19}Y_{0.3}$ bond coat alloy following oxidation for 500 h at 1100 °C (a) sign of initial stages showing oxidation above β- and γ-phases (b) a highlighted area of the microstructure shown in (a), and (c) growth of spinel protruding above the surface at certain locations. Needle-like oxides surrounding these could be the initial growth of θ-Al_2O_3, which later converted to spinel without losing the shape [47,48,54].

that is diffused from Al-rich bond coat alloys. Fig. 12(a) presents the BSE micrograph of Pt-free bond coat alloy diffusion coupled with CMSX-4 superalloy after annealing at 1100 °C for 64 h. The microstructure reveals that the IDZ comprises two distinctive zones grown differently from the bond coat and the superalloy, as indicated by the position of the Kirkendall marker plane (K) marker plane, evident by the presence of line pores, which is one of the reliable methods for detecting the position of K plane without using inert particle [46]. This plane's position helps to understand the growth process from the two opposite interfaces differently. From the bond coat (a phase mixture of γ and β-phases), a sublayer of γ-phase grows because of the loss of Al from the β-phase. IDZ grows differently from the superalloy, i.e., by losing Ni from the superalloy and by adding Al, which is dissociated and diffused from the other interface. It grows with two different sublayers: a TCP containing γ+γ' phase mixture and another precipitate-free γ phase. Therefore, a sublayer of the γ-phase grows on both sides of the bond coat by the growth of the IDZ (Fig. 12) and oxide layer (see Fig. 5).

The presence of γ+γ' phase mixture in the precipitate-containing zone may not be clear from Fig. 12(a). The STEM-EDS composition analysis in this zone, as shown in Fig. 13, clearly indicates the presence of a two-phase mixture: γ-Ni(Al,x) solid solution phase is relatively Ni-rich, whereas the γ'-$Ni(x)_3Al(x)$ phase is relatively Cr-rich. The TCP precipitates are identified by relatively higher W and Re concentrations than the matrix. The difference between matrix and precipitates is not so high for Ta and Mo. A TEM analysis was conducted to structurally characterize TCP precipitates in IDZ. Cross-sectional TEM samples were prepared from IDZ of bond coats-CMSX-4 superalloy. Fig. 14 shows the bright-field micrograph from the TCP phases grown in NiCrAl-CMSX-4 superalloy. The SADP suggests that two different TCP phases, R and μ phase, grow in γ' matrix. The diffraction pattern from the R and μ phases

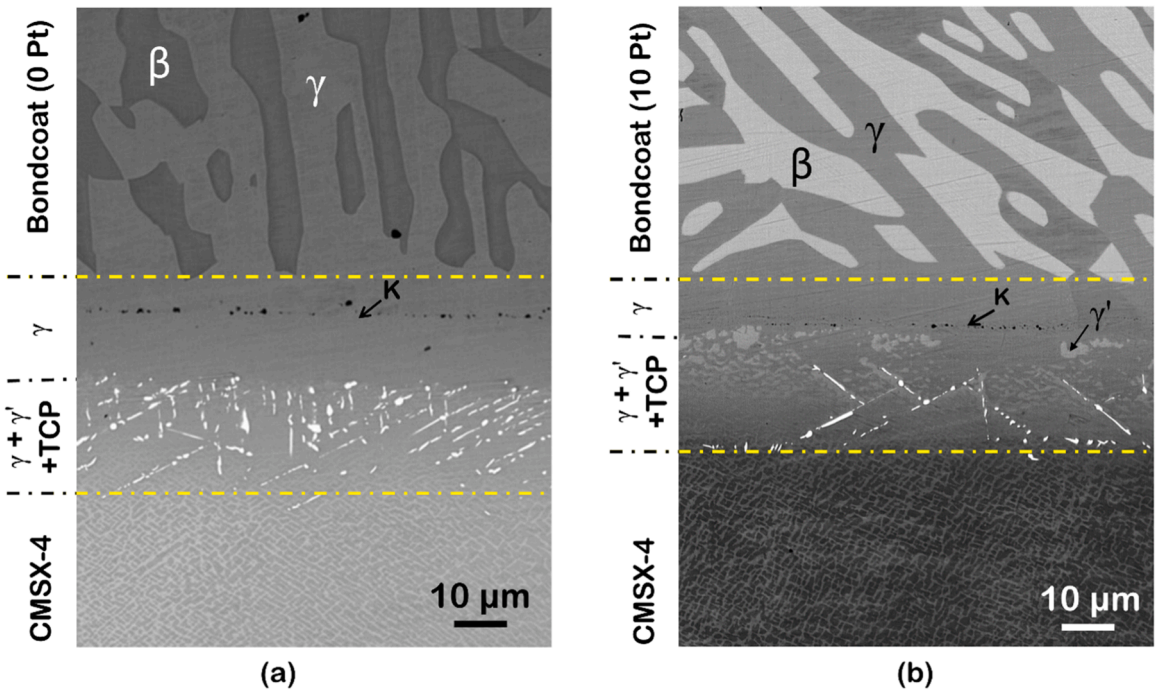

Fig. 12. : Inter-diffusion zone between bond coat (a) $Ni_{59.3}Cr_{21.7}Al_{19}$, (b) $Ni_{49.3}Cr_{21.7}Al_{19}Pt_{10}$ (10 Pt) and CMSX-4 superalloy annealed at 1100 °C for 64 h. The Kirkendall marker plane is indicated by the "K".

indexed to the rhombohedral crystal structure, with space groups R-3 and R-3m, respectively. The STEM-EDS compositions of the γ, γ' and TCP phases are listed in Table 3. Moreover, the precipitates are found in the γ' phase (see Fig. 13), which is relatively rich in Ni but lean in Cr compared to the γ-phase in the IDZ, which can be understood from the composition of the phases.

The effect of Pt addition to bond coat on the growth of IDZ is evident from Fig. 12(b). With the increase in Pt content in bond-coat alloys, the growth mechanism of the phase layers remains similar (although not the thickness of IDZ). The thickness of total IDZ is measured to be 33 ± 2 μm in the presence of Pt, which is decreased from 43 ± 2 μm that is grown in the absence of Pt in the bond coat. The growth characteristics of the γ phase from the bond coat, i.e. the IDZ sublayer on the right-hand side of the Kirkendall marker plane, remain similar with a very small difference in thickness. However, a significant difference in the characteristic of IDZ growth from the superalloy is found, including a reduction in the volume fraction of precipitate in the γ+γ' phases and a significant reduction in the thickness of the γ-phase grown from the superalloy. The thickness of this part of the γ phase is so small that the K plane's location is very close to the precipitate containing the γ+γ'-phases. Further, the notable contrast inversion of γ and γ' phases in IDZ compared to the superalloy is evident. The presence of the phase mixture in the precipitate-containing zone can be seen evidently in the STEM-EDS composition map, as shown in Fig. 15. The partitioning of composition in these two phases is listed in Table 4. The higher concentration of Mo, Ta, W, and Re dissolved in γ phase in superalloy results in brighter contrast in the BSE micrograph (Fig. 12(b)), which is reversed by reduction of the concentration of these elements for the growth of precipitates and because of a little higher concentration of Pt in the γ'-phase compared to the γ-phase in IDZ. The TEM analysis on these two phases, as shown in Fig. 16, confirms the above interpretation. Therefore, there is a reduction in the total thickness of IDZ by the addition of Pt and also a significant decrease in the volume fraction of precipitates (compare Figs. 12(a) and 12(b)). The fraction of TCP precipitates is measured to be 0.2 in the presence of Pt in the bond coat compared to 0.67 in the absence of Pt although no difference was found in the types of precipitates for Pt-free and Pt-containing bond coats.

4. Discussion on the effect of Pt on the growth mechanism of oxide, spallation resistance and the growth of the interdiffusion zone

4.1. Oxidation mechanism

NiCrAlY-type overlay coatings benefit from positive mechanical properties due to the presence of both β (relatively brittle) and γ (relatively ductile) phases compared to the diffusion coating, which is mainly comprised of the β-phase. The need to develop good oxidation-resistant material without compromising the mechanical properties led to developing a multi-component MCrAlY coating with a two-phase mixture. The need to grow a continuous alumina layer with relatively low Al content is fulfilled by adding Cr. For example, adding 5–10 at% Cr reduces the need for Al content from 40 to only 10 at% [61]. Y is added to reduce severe oxidation degradation by producing an adherent oxide layer. As demonstrated in this study, adding Pt further improved the adhesion. It also helped reduce the unwanted loss of Al by decreasing the growth of the precipitate-containing interdiffusion zone. The ultimate purpose of this type of coating layer is to grow a continuous α-Al_2O_3, which is considered the most important oxide phase for the protection of substrate because of very low diffusion rates of Al and oxygen. However, multiple elements (depending on composition) and dual phases lead to a complex growth of more than one oxide phase and even the products of oxides (such as $YAlO_3$ and spinel). Moreover, the dynamic redistribution of elements adjacent to the bond coat may lead to sequential instead of simultaneous growth of the oxides [8,62–64].

The growth characteristics of the oxide layer on a metallic substrate are expected to be controlled by the average alloy compositions and phases, diffusion rates of elements in the substrate, the oxide phases, thermodynamic conditions, experimental conditions, etc. For example, the initial oxidation process can be different at different phases (β and γ), similar to the present example, as shown in Fig. 11 (a and b). With the loss of Al, the β-phase converts to the γ-phase and then the oxide layer grows on the γ-phase only, as shown in Fig. 5. Initially, there is a possibility of growing all the active elements (Ni, Cr, Al and Y in this case). However, the possibility of finding a particular oxide (Al_2O_3) and/or

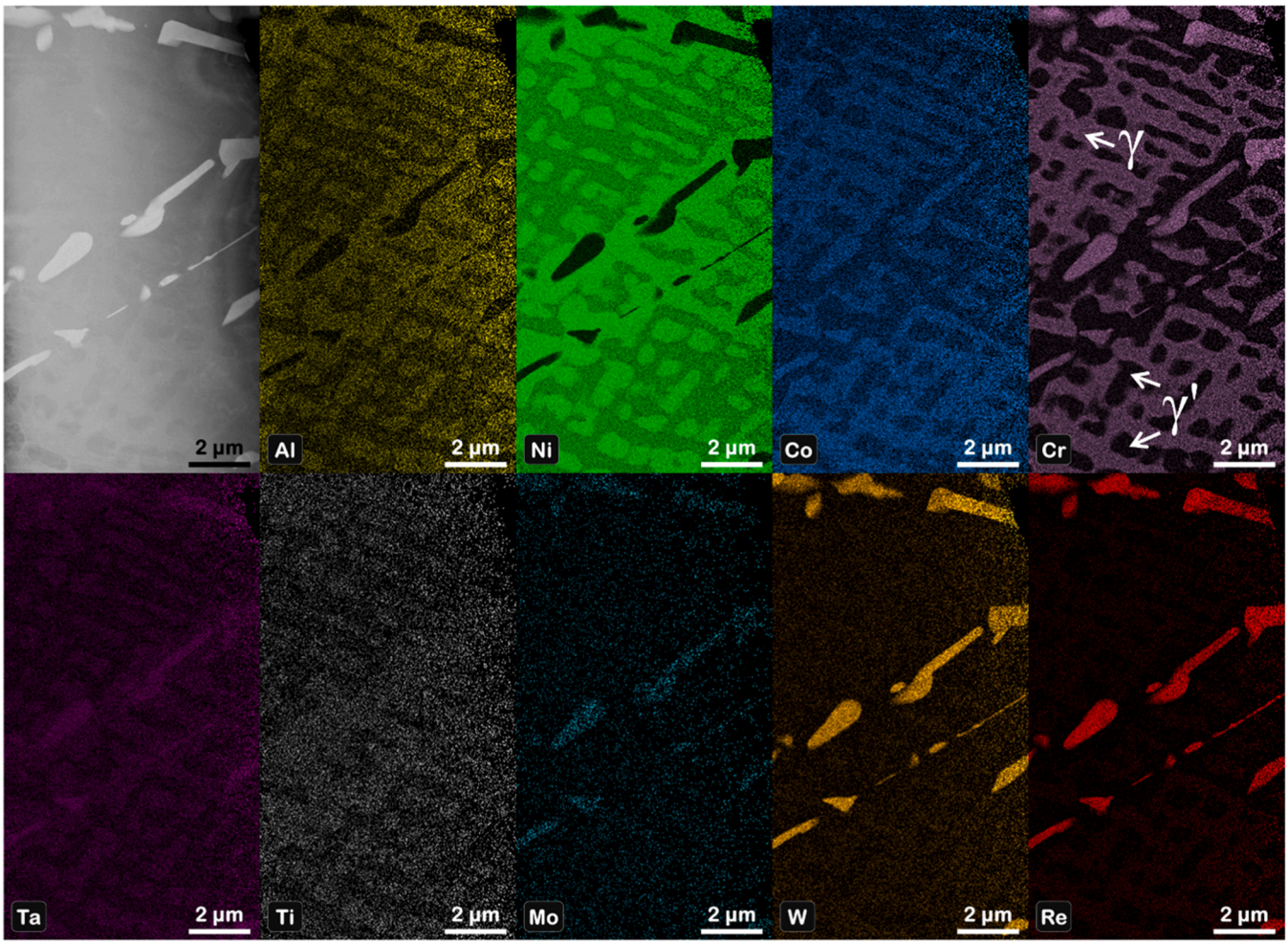

Fig. 13. : STEM-EDS maps of the elements from the precipitate containing interdiffusion zone (IDZ) in CMSX-4/bond-coat NiCrAl (0 Pt) alloy. The TCP precipitates are found to grow in γ' phase. The Cr-map highlight regions with higher Cr as γ and those with lower Cr as γ'.

several other oxides (NiO, Cr_2O_3 and Y_2O_3) depends on the alloy composition and oxidation condition. Moreover, a product of two different oxides (such as $YAlO_3$ and spinel in the present study) may also be found (which is the case in this study). Nijdam et al. [44,65] have explained the oxidation mechanism of γ-NiCrAl with an average composition close to the composition of the γ'-phase (without Y and Pt) in similar oxidation conditions, i.e. 1100 °C and oxygen partial pressure of $2 \times 10^4 Pa$ similar to the partial pressure of oxygen in the air. This sheds light on the overall oxidation process. However, the growth of the oxide phases is far more complex in the present study because of the presence of both β- and γ-phases with very different average substrate compositions in the presence of additional elements Y and Pt.

The growth of oxides of active elements (let's say M^1, M^2, M^3, etc.) in an alloy from a particular phase can be expressed as [44]

$$\frac{2i}{j}M^n + O_2 = \frac{2}{j}M_i^n O_j \tag{1}$$

Where $n = 1, 2, 3$ etc. The local equilibrium of the oxide phase with the substrate is related to the equilibrium partial pressure of oxygen (P_{O_2}) by

$$P_{O_2}(M_i^n O_j) = \frac{a_{M_i^n O_j}^{\frac{2}{y}}}{a_{M^n}^{\frac{2i}{j}}} \exp\left(\frac{\Delta G^o_{M_i^n O_j}}{RT}\right) \tag{2}$$

where $a_{M_i^n O_j}$ and a_{M^n} are the activities of oxide and metal species in the alloy. $\Delta G^o_{M_i^n O_j}$ is Gibb's energy of formation. Neglecting the solubility between different oxides, the activity of an oxide phase can be considered as one, and the metal species' activity is related to the concentration in the alloy. Further, there is a possibility of finding a reaction product of different oxide phases, such as $M^1M^2O_3$ ($YAlO_3$ in the present example), and $M_1(M_2)_2O_4$ (different types of spinel such as $NiCr_2O_4$, and $NiAl_2O_4$, $Ni(Al,Cr)_2O_4$ etc. in the present study) instead of individual oxide phases. If we neglect the presence of the product of different oxides, whether a particular oxide (let's say NiO, Y_2O_3, Al_2O_3 or Cr_2O_3) or more than one oxide will be found depends on the equilibrium partial pressure at the interface at a particular temperature and partial pressure of oxygen for a given alloy composition.

The Gibbs energy of the formation of Y_2O_3 is higher (more negative) among all oxides and, therefore, the first to form at the substrate oxygen interface [25]. As discussed already, Y dissociates from Ni_5Y present in the substrate for the growth of Y_2O_3. The diffusion of oxygen through Y_2O_3 then induces the formation and growth of Al_2O_3, which is the next most stable oxide [23]. As reported by Nijdam et al. [44], Al_2O_3 is favorable to grow in the presence of as low as one ppm of Al in Ni-27Cr alloy, irrespective of oxygen partial pressure. With the loss of Al, Cr concentration increases at the substrate/oxide interface, and Cr_2O_3 is the next stable oxide phase to grow. With the loss of Al and Cr, the concentration of Ni may increase to a level such that NiO may grow. However, as already described, other oxides, except Al_2O_3 and Cr_2O_3, are not found individually, which can be explained.

The overall growth of major oxides is shown in the schematic diagram in Fig. 17. As shown in Fig. 1, Y-containing Ni_5Y intermetallic

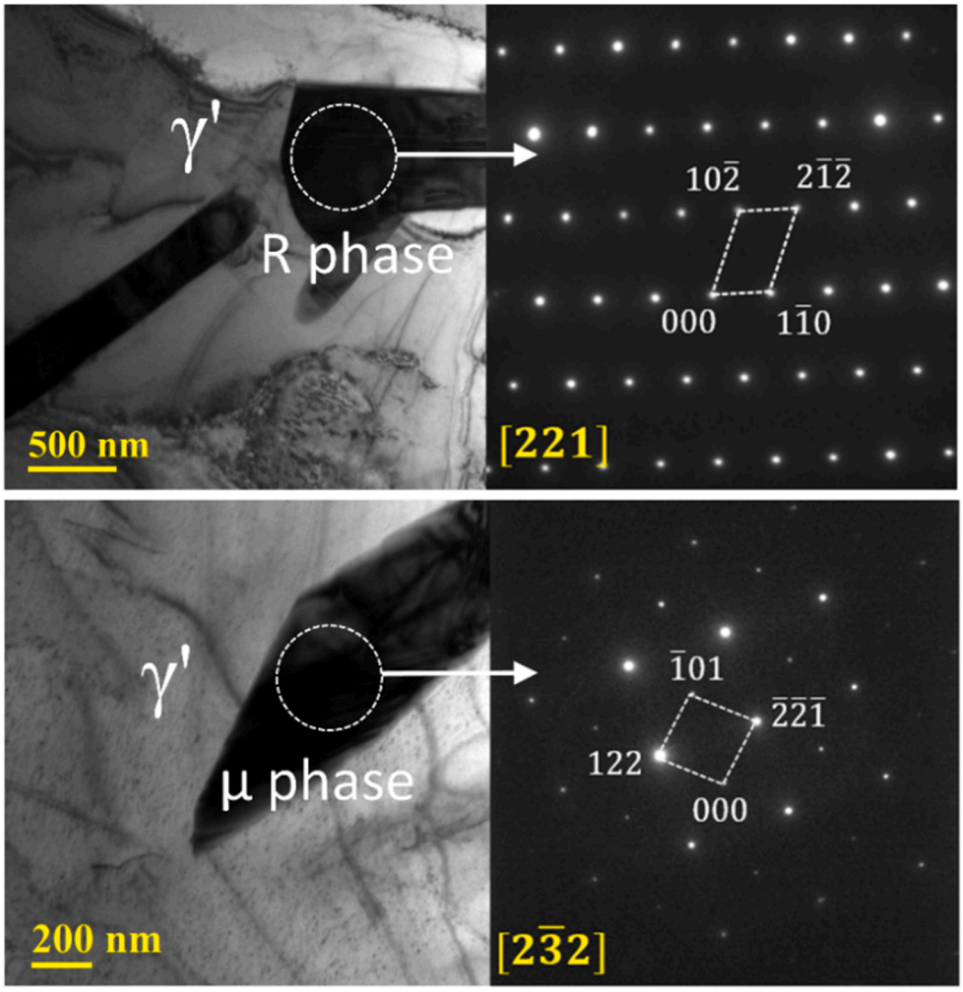

Fig. 14. : Bright field TEM micrograph with their corresponding diffraction pattern of the TCP precipitates formed in the $Ni_{59.3}Cr_{21.7}Al_{19}$/CMSX-4 diffusion couple annealed at 1100 °C for 64 h.

Table 3
STEM-EDS composition analysis of the γ', γ, μ and R phases in the interdiffusion zone (IDZ) of CMSX-4/bond-coat $Ni_{59.3}Cr_{21.7}Al_{19}$ alloy diffusion couple.

Elements (at%)	Ni	Al	Co	Cr	Mo	Ta	Ti	W	Re
γ'	69.9 ± 2.2	9.2 ± 1.8	5.8 ± 0.6	5.3 ± 0.7	0.5 ± 0.3	5.2 ± 0.4	1.6 ± 0.3	1.9 ± 0.4	0.6 ± 0.2
γ	56.8 ± 1.3	5.5 ± 0.8	8.0 ± 0.91	21.5 ± 0.1	0.8 ± 0.5	3.4 ± 0.4	0.9 ± 0.3	2.1 ± 0.2	1.0 ± 0.1
μ phase	16.4 ± 0.7	3.2 ± 0.8	9.9 ± 0.6	26.4 ± 0.8	3.0 ± 0.7	9.4 ± 0.6	1.7 ± 0.3	19.4 ± 0.9	10.6 ± 0.9
R phase	13.7 ± 2.3	4.0 ± 1.2	6.1 ± 1.4	32.6 ± 2.0	2.7 ± 1.2	8.7 ± 1.5	1.6 ± 0.6	15.1 ± 2.1	15.5 ± 1.0

compounds are present at the γ/β interface, which acts as the source for Y for the growth of Y_2O_3. This oxide is more favorable to grow when this compound is exposed to oxygen [25]. Al_2O_3 is favorable to grow subsequently since this is the next most stable oxide, which can grow with the very low partial pressure of oxygen at the metal/oxide interface. For example, only one ppm Al in Fe-27Cr alloy is favourable to growing Al_2O_3 [44,65]. A relatively high concentration of Al leads to the growth of Al_2O_3 with a higher fraction. A certain fraction of alumina is reacted immediately to Y_2O_3 in equimolar composition (see Ref. [66]) to develop the product of these two oxides as $YAlO_3$ pegs found at the substrate/oxide interface. Moreover, oxygen can diffuse through the grain boundaries. Additionally, oxygen solubility is relatively higher in the γ- compared to the β-phase, and these oxides grow in the bond coat at the β/γ interface [44,45]. Subsequently, β-converts to γ-phase with the loss of Al and the oxide grows on the γ-phase only. However, the channel of $YAlO_3$ indicates the original interface between the phases, as shown in Fig. 17(b). A very similar growth pattern of a different Y- and Al-containing oxide ($Y_3Al_5O_{12}$) was reported in Ref. [66], which grew at the grain boundaries of a single phase of FeCrAlY alloy because of the presence of Y-containing intermetallic at the grain boundaries [25].

At the initial stage, the growth of the oxide layer is found to be different based on the growth above the γ- or the β-phases (Fig. 11), which is also shown in detail by Chen et al. [8]. The surface roughness of the oxide phase on the β-phase is higher. It is already known that only alumina grows with ridge structure on β-NiAl and β-Ni(Pt)Al coating alloy, as shown in the supplementary file Fig. S2. This experiment is conducted for 1000 h at 1100 °C compared to 500 h for NiCr(Pt)AlY bond coats since this has only α-Al_2O_3 oxide layer with a much smaller thickness compared to mixed oxide on NiCr(Pt)AlY with higher thickness. A similar ridge-type structure is also initially found to grow on the β-phase of NiCr(Pt)AlY overlay coating alloy. The ridge structure results from a higher growth rate of the oxide phase above the grain boundaries because of the higher diffusion rate of Al compared to the growth rate above the grain by the lattice diffusion [17]. Moreover, as shown in

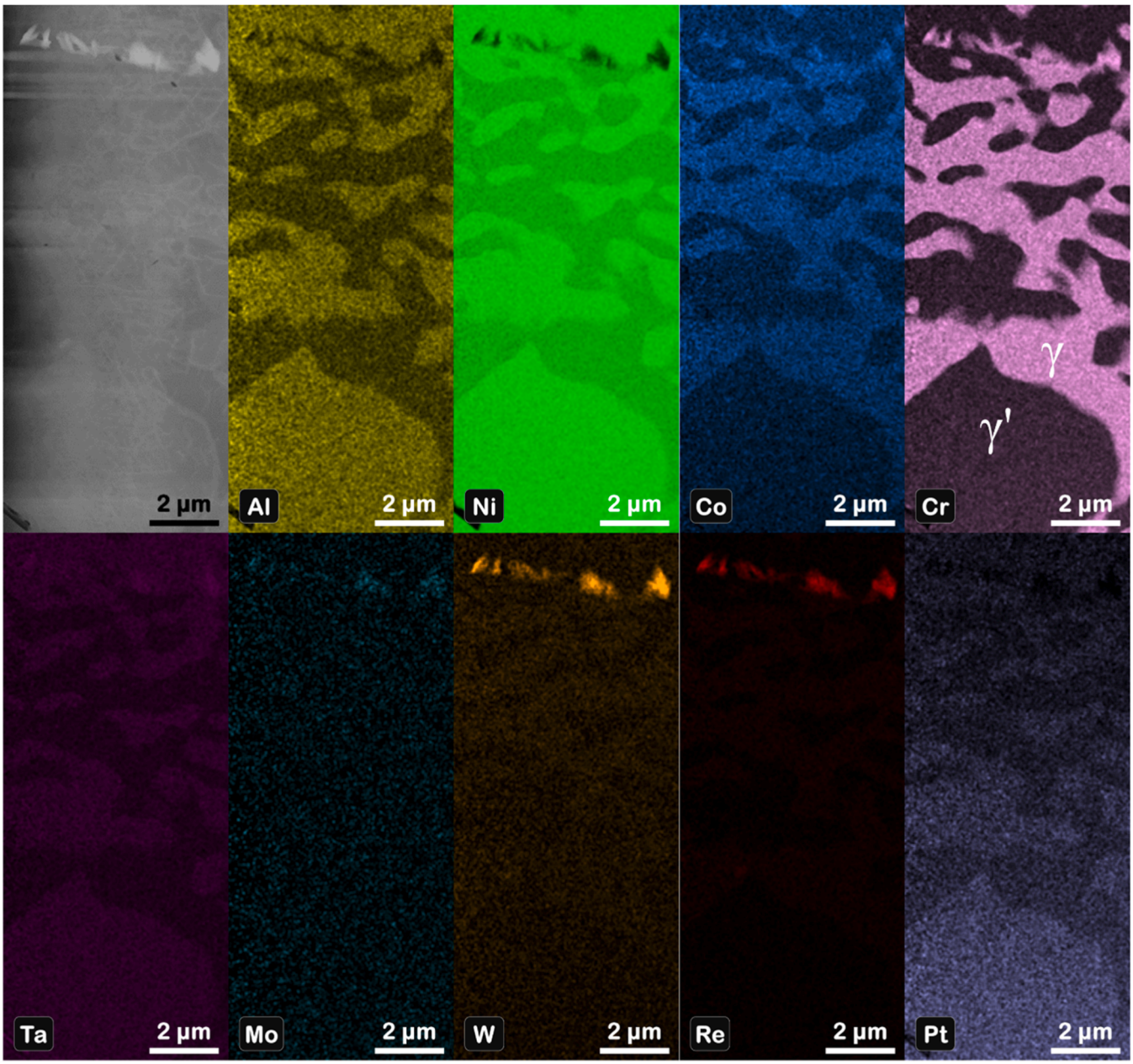

Fig. 15. : STEM-EDS maps of all elements from the interdiffusion zone (IDZ) in CMSX-4/ $Ni_{49.3}Cr_{21.7}Al_{19}Pt_{10}$ show precipitate-containing γ and γ' phases (marked in Cr map). TCP precipitates are found to grow in the γ' phase.

Table 4
STEM-EDS composition analysis of the γ' and γ in the interdiffusion zone (IDZ) of CMSX-4/bond-coat $Ni_{49.3}Cr_{21.7}Al_{19}Pt_{10}$ alloy diffusion couple.

Elements (at%)	Ni	Pt	Al	Co	Cr	Mo	Ta	Ti	W	Re
γ'	64.2 ± 1.8	3.6 ± 0.2	10.5 ± 0.6	3.7 ± 1.1	6.0 ± 1.3	0.9 ± 0.2	7.1 ± 0.4	1.5 ± 0.3	1.8 ± 0.2	0.7 ± 0.1
γ	54.0 ± 0.6	1.5 ± 0.2	5.7 ± 0.3	6.7 ± 0.5	21.7 ± 0.3	1.0 ± 0.2	5.0 ± 0.2	1.0 ± 0.2	2.0 ± 0.2	1.4 ± 0.1

Fig. 11(c), the needle-type structure is also found to grow at certain locations, which have typical characteristics of θ-Al_2O_3 at the initial stage of oxidation but transform to the most stable α-Al_2O_3 afterwards [8,42]. The oxide surface over the γ-phase is not that rough (but faceted) because of the growth of Cr_2O_3 and spinel on the top [8]. After the very initial stage, the β-phase converts to the γ-phase with the loss of Al from the β-phase. The experiment of Chen at 1150 °C indicates this transformation to happen at the substrate adjacent to oxide within 5 min [8]. The diffusion rate in the substrate γ-phase compared to the diffusion rate of elements through oxide is much higher. Therefore, the substrate reaches compositional homogeneity in the γ-phase substrate such that the oxidation process becomes similar over the whole substrate. Cr_2O_3 and NiO grow at the oxide/air interface by diffusion of Cr and Ni through the oxide. In our study, similar to studies reported earlier, we found that $NiAl_2O_4$ and $Ni(Al,Cr)_2O_4$, which indicates the reaction of NiO and Cr_2O_3 with Al_2O_3 on the top of the oxide layer for the formation of spinel [50–53,57]. A rough top surface is believed to be created because of the transformation of θ-Al_2O_3 to α-Al_2O_3 (with a reduction in

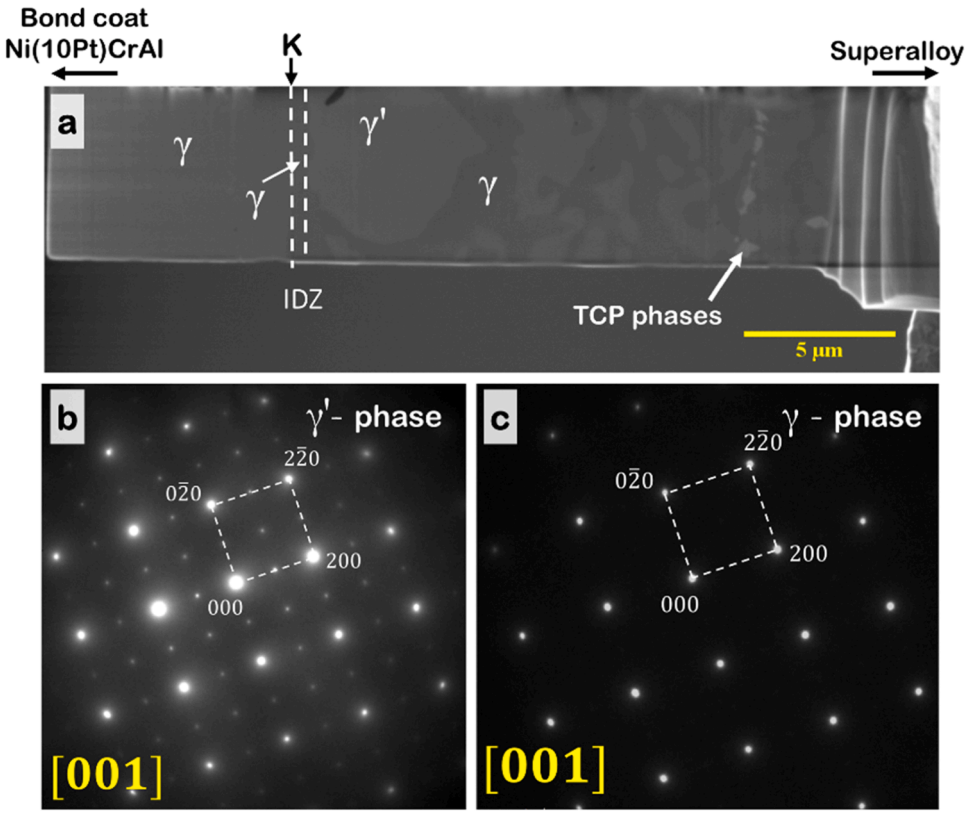

Fig. 16. : Cross-section micrograph showing the $Ni_{49.3}Cr_{21.7}Al_{19}Pt_{10}$ bond coat and interdiffusion zone (IDZ) interface. The bright phase observed in the IDZ is depicted to be γ' and TCP formed in the γ-phase.

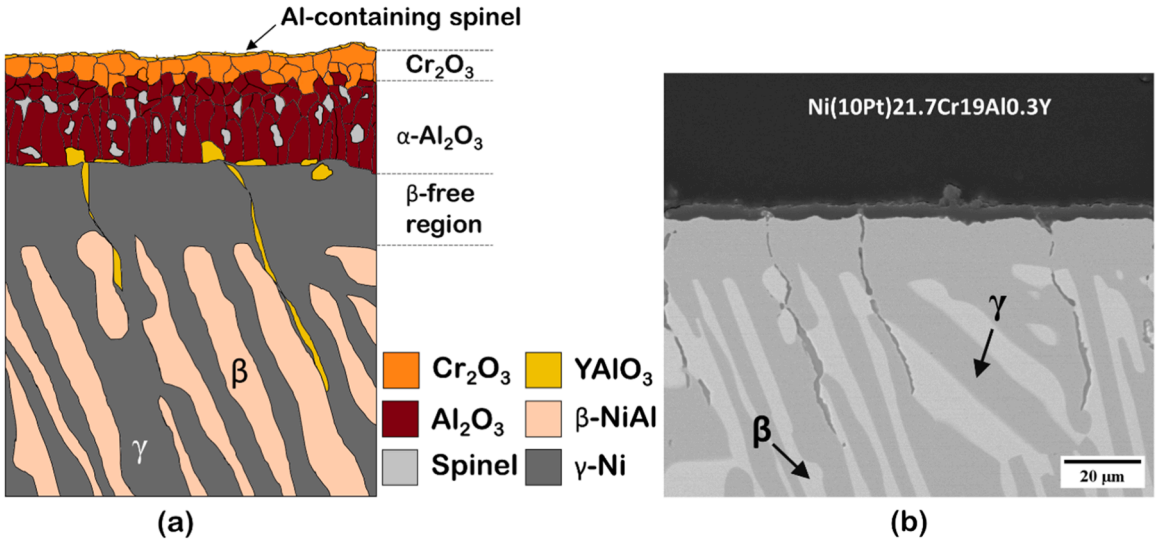

Fig. 17. : (a) A schematic illustration of the oxide microstructure resulting from the oxidation of $Ni_{49}Pt_{10}Cr_{21.7}Al_{19}Y_{0.3}$ bond coat alloy. (b) Growth of $YAlO_3$ inside the bond coat substrate after isothermal oxidation of (Ni,Pt)AlCrY.

volume significantly), the transformation from Al_2O_3, NiO (and Cr_2O_3) to $NiAl_2O_4$ (and $Ni(Al,Cr)O_4$) and even evaporation of Cr by forming CrO_3 [50]. These oxide phases are known to grow outwards with higher rates and act as the source of failure by producing cracks when YSZ (yttria-stabilized zirconia) is deposited at the top for thermal protection [51–53,57].

Fig. 7 notably highlights a duplex grain morphology of α-Al_2O_3, a common characteristic observed even on β-Ni(Pt)Al bond-coat alloys [17]. The plane demarcating these distinct grain morphologies, i.e. long grain (LG) and short grain (SG), in Fig. 7 corresponds to the position of the Kirkendall marker plane. The position of this plane indicates that the sublayer with long grains is grown from the sublayer because of the diffusion of oxygen through the oxide phase. On the other hand, the sublayer with the short columnar grains is grown from Cr_2O_3 or air by the diffusion of Al. The measured ratio of the thickness of the inner coarse columnar grain layer to the outer layer with finer equiaxed grains is determined to be 2.9 ± 0.5. A similar ratio was also reported in our earlier study [17]. This indicates that a relatively thin but continuous

layer of Cr_2O_3 and other discrete spinel oxide phases do not change the overall growth mechanism of the α-Al_2O_3 phase. The sequence of the oxide phase growth between the bond coat and oxygen in air could be explained with the help of the diffusion path when the multicomponent phase diagram, along with the solubility range of phases and thermodynamic details, are known following the rules proposed by Kirkaldy and Brown [67,68], compiled by Clarke [69] with the help of available thermodynamic details. However, this cannot be discussed further in this system because of the unavailability of these details.

4.2. Spallation resistance

To understand the spallation resistance of the oxide, we need to discuss the role of Y and Pt. As already discussed, the occurrence of oxide pegs ($YAlO_3$) is intrinsically related to the Y concentration within the alloy. The formation of $YAlO_3$ oxide at the oxide/bond-coat interface not only modifies the growth rate of Al_2O_3 but also enhances the adhesion due to the formation of oxide pegs. The inward growth of the Al_2O_3 layer effectively incorporates $YAlO_3$ oxides, as evidenced by Fig. 10. Prolonged exposure to high temperatures results in the continued inward growth of the Al_2O_3 layer, which, in turn, reduces the number of oxide pegs at the interface, resulting in a more planar oxide layer interface, ultimately leading to spallation. The role of oxide pegs at the interface on spallation resistance is well-documented [23,25,38,55,56]. The increase in the oxide growth rate because of Y addition is believed to be due to the fast diffusion path of elements by the growth of Y-containing oxide [24]. The addition of Pt did not change the growth rate of the oxide phase. Pt is not found in the oxide layer to influence the oxidation process. It also indicates that Pt does not significantly influence the driving force for oxide growth. However, it may have improved the adhesion strength between the bond coat and oxide to reduce the spallation resistance. The adherence of the oxide layer is remarkably enhanced in the presence of both Y and Pt. The addition of Pt on the increase in spallation resistance of the oxide scale on the β-NiAl bond coat is well known even in the absence of the S-containing environment [17]. This indicated a possible change in the diffusion mechanism of elements in the substrate suppressing the growth of (Kirkendall) voids at the oxide/substrate interface and possibly also increasing oxide adherence strength to the substrate. The Kirkendall voids are unlikely to grow at the γ-phase/oxide interface since Al has higher diffusion rates than Cr and Ni in this Ni-based solid solution [70,71]. The consumption of Cr and Ni is far less for the growth of Cr_2O_3 and spinel. Therefore, vacancies flow away from the bond coat/oxide interface when Al diffuses out for the growth of the oxide phases. Indeed, Kirkendall voids were not located in this study on Ni(Pt)CrAlY bond coat alloys at the substrate/oxide interface (the presence of which is not reported in articles available in the literature as well). This indicates a possible role of Pt in increasing the adhesion strength of oxide with substrate. These aspects are further discussed in detail in the next section. The growth rate of the oxide layer, comprised of only α-Al_2O_3 on β-NiAl and Ni(Pt)Al diffusion coating alloys, is found to be less (annealed for 1000 h, see Fig. S2a) than overlay coating Ni(Pt)CrAlY coating (annealed for a maximum of 500 h, as shown in Fig. 5) because of the presence of other non-protective oxides with higher diffusion rates of elements (i.e. higher growth rate). The increase in spallation at higher oxidation times, followed by cooling, is most likely a straightforward consequence of the increasing strain energy stored as the oxide layer thickens. While there have been reports of stress relaxation in oxides forming on thin bond coats, especially at higher temperatures [72], the substrate thickness here (1.5 mm) precludes any significant relaxation at 1100 °C.

4.3. The growth mechanism of the interdiffusion zone in the absence and presence of Pt in the NiCrAl bond coat

It has already been demonstrated in this article that the interdiffusion zone thickness and fraction of precipitates decrease with the addition of Pt. Although the difference in the thickness of the sublayer that is grown from the bond coat does not change much (right-hand side of the marker plane in Fig. 12), a significant difference is found in the overall thickness of the sublayer that is grown from the superalloy (left-hand side of the marker plane). This sublayer has two parts: a precipitate containing γ+'' phase mixture and a precipitate-free γ phase. With the addition of Pt in the bond coat, the thickness of the precipitate-containing γ+γ' phase mixture part decreases slightly; however, the thickness of the precipitate-free γ phase layer decreases drastically such that the distance between the precipitate-containing part and the Kirkendall marker plane is very small.

The superalloy is a phase mixture of ~ 37 % γ and ~ 63 % γ'. Without Pt in the bond coat alloy, the precipitate-containing phase mixture grows with ~ 49 % γ, ~ 45 % γ' and ~ 6 % precipitates. Therefore, the fraction of γ increases and γ' decreases. Further, the precipitate-free γ also grows next to it. This part grows by the diffusion of elements such as Ni, Co, Cr, Al, and Ta, which have higher diffusion coefficients and, therefore, lean in Re and W content, which have much lower diffusion coefficients [73,74], as confirmed by the composition analysis of the precipitate-free γ phase. During this overall conversion of γ' to γ, the TCP precipitates with high content of Re and W grow inside the γ' phase because of much lower diffusivity than the other elements. In the presence of Pt in the bond coat, the fractions of γ and γ' phases i.e. ~ 41 % γ and ~ 57 % γ' are not very different from the fractions of these phases in the superalloy. However, since the growth of the precipitate-free zone (which grows by diffusing the faster diffusing elements such as Ni, Co, Cr, Al, Ta, etc. and by rejecting the slower diffusing elements such as Re and W) reduces drastically, the overall fraction of TCP precipitates is also significantly less.

The diffusion path sheds further light on the growth sequence of the phases. The practice of drawing the diffusion paths can be learnt from Refs [67–69,75–77]. It should be noted here that we cannot represent a multi-component system in a ternary Ni-Al-Cr for such a discussion accurately, and, therefore, this should be considered as a qualitative argument for understanding the overall composition variation of the interdiffusion zone. The phase diagram in Fig. 18 is extracted from the TCNi9 dataset of ThermoCalc [78–80]. A red-filled circle indicates the average composition of the superalloy, and the orange-filled circle indicates the bond coat alloy. Let us consider the growth of the

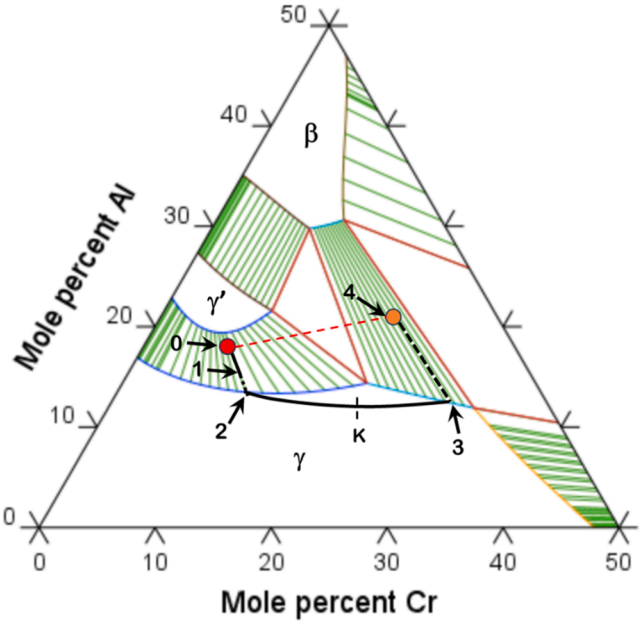

Fig. 18. : Diffusion path of the interdiffusion zone between the bond coat and superalloy.

interdiffusion zone between the superalloy and Pt-free bond coat, as shown in Fig. 18. From the superalloy, the same phase mixture of γ and γ' grows but with decreasing phase fraction of the γ' and increasing phase fraction of the γ, *i.e.* from 0 to 1 in Fig. 18. The transition from the phase mixture to the single-phase γ is represented by the dotted line between 1 and 2. The diffusion path between 2 and 3 represents the composition variation of the precipitate-free IDZ on both sides of the marker plane (K). The interface between IDZ and the bond coat is represented by the dotted line between 3 and 4. Since the interfaces between different sublayers are more or less straight with end members, the dotted lines are drawn parallel to the two-phase equilibrium region's tie lines (iso-activity) lines [67–69]. Further, it must be clear from the diffusion paths that Cr has a typical downhill diffusion from one end to another (i.e. a decrease in Al content from the bond coat end to the superalloy end). However, Al goes through uphill diffusion in which Al content first decreases and then increases, although the composition is always lower than the variation along the (red dashed) line connecting the end members. Further, it should be noted that the diffusion path on the Gibbs triangle indicates only the composition profile but not the thickness of the interdiffusion zone length. Uphill diffusion reduces interdiffusion zone length compared to the downhill diffusion of all the elements depending on the diffusion direction of elements [77,81]. The main difference in the interdiffusion zone in the presence of Pt in the bond coat is found in the reduction in the thickness of the precipitate-free interdiffusion zone grown from the superalloy. An interdiffusion study indicates a marginal reduction in main interdiffusion coefficients of Al ($\widetilde{D}^{Ni}_{AlAl}$) with the addition of Pt in γ-Ni(Al,Pt) solid solution [82]. The main interdiffusion diffusion coefficient of Pt ($\widetilde{D}^{Ni}_{PtPt}$) is much smaller. Further, the cross interdiffusion coefficients of Al which is related to the concentration gradient of Pt ($\widetilde{D}^{Ni}_{AlPt}$) is negative. This implies that when Al and Pt are forced to diffuse towards the same direction (i.e. from Al- and Pt-rich bond coat alloy), the downhill diffusion of Pt will increase the uphill diffusion of Al. The characteristics of diffusion profiles at different composition ranges can be different depending on the thermodynamic parameters. This increase in Al uphill diffusion results in a decrease in interdiffusion zone length and, therefore, unwanted loss of Al.

4.4. A comparison of oxide spallation and evolution of interdiffusion zone between β-Ni(Pt)Al and (γ + β)-Ni(Pt)CrAlY alloys

As explained in Ref. [17], Kirkendall voids grow at the substrate-oxide interface in bond coat alloy with stoichiometric composition β-NiAl, as shown in Fig. S3. As Al is consumed from the bond coat alloy for the growth of alumina, Ni concentration increases in the substrate adjacent to the bond coat/oxide interface (shifting the composition towards Ni-rich alloy of β-NiAl). This leads to the diffusion of Ni in the opposite direction (i.e. away from the substrate/oxide interface). Since Ni has a higher diffusion rate than Al in this composition range of the Ni-rich β-NiAl phase [83,84], vacancies flow towards the substrate/oxide interface. These grow as Kirkendall voids, as shown in the supplementary Fig. S3. The voids in the substrate could be found easily after the spallation of oxide above them. The growth of voids is known to be one of the major reasons for failure. Brumm and Grabke [85] have shown that these voids grow on Ni-rich NiAl alloy as well (similar to the stoichiometric composition explained in this study). These did not grow on the Al-rich β-NiAl alloys since the diffusion rate of Al is much higher compared to Ni [83,84].

Various factors of the beneficial role of Pt addition in the β-NiAl coating are well documented [16,86,87]. We discuss only a few salient features in this to compare the role of Pt in NiCrAlY coating. The addition of Pt possibly changes the diffusion rates of elements such that voids are not found at the β-Ni(10Pt)50Al/oxide interface during the growth of oxide [17]. The measurement of the pseudo-binary interdiffusion coefficient of Ni and Al ($\widetilde{D}_{PB}$) indicates an increase in interdiffusion coefficient with the increase in Pt content [19,21,22]. The measurement of the ternary diffusion coefficient at 1100 °C in the Ni-rich Ni-Pt-Al ternary system indicates that the main interdiffusion coefficient of Ni ($\widetilde{D}^{Pt}_{NiNi} = 8.5 \times 10^{-15} \quad m^2/s$) is less than the main interdiffusion coefficient Al ($\widetilde{D}^{Pt}_{AlAl} = 42.5 \times 10^{-15} \quad m^2/s$) considering Pt as the dependent variable (see the supplementary file of Ref. [20]). Bouchet and Mevrel also indicated the increase in Al diffusion coefficient with Pt addition [88]. The role of Pt on thermodynamic parameters benefitting the favorable Al diffusion is well documented [89–91]. Moreover, both the cross-interdiffusion coefficients ($\widetilde{D}^{Pt}_{NiAl} and \widetilde{D}^{Pt}_{NiAl}$) are found to be negative, indicating increased flux of both Ni and Al when diffused in opposite directions (with opposite signs of composition gradient). In such a situation, the flux of Al towards the bond coat/oxide interface may be higher compared to Ni (and Pt) in the opposite direction, leading to the flow of vacancies away from the substrate/oxide interface. This must be why the Kirkendall voids could be found during the oxidation of β-Ni50Al but not β-Ni(10Pt)50Al to improve the spallation resistance. Additionally, it is possible that the adhesion strength of the oxide layer also improves the spallation resistance by adding Pt since spallation resistance improves even in air without an S environment [17]. The role sulphur segregation on spallation resistance of oxide is well documented [11–16]. However, the role of sulphur segregation is beyond the scope of this article and, therefore, not discussed extensively.

As already explained, oxide grows differently over the β- and γ-phases at the very early stage of oxidation on (β+γ)-NiAlCrY bond coat alloys. With the loss of Al, the β-phase starts converting to the γ-phase within a few minutes of oxidation, with the loss of Al consumed for alumina growth [8]. The interdiffusion coefficients calculated in the β-NiCrAl phase by Hou et al. indicate similar main interdiffusion coefficients compared to those in the binary β-NiAl system [92]. The interdiffusion coefficients are a kind of average of intrinsic diffusion coefficients of elements and may not reflect the relative mobilities of the species (of intrinsic flux) correctly. Still, we can make a qualitative discussion based on the main interdiffusion coefficients of the ternary system since the cross-intrinsic diffusion coefficients are found to be very small in this ternary system [92]. We may consider a similar rate and process of interdiffusion of elements since the ternary main interdiffusion coefficients in the β-NiCrAl phase because of Cr addition are similar to the binary interdiffusion coefficient in the β-NiAl phase. Therefore, voids may grow at the Ni-rich β-Ni(Cr)Al phase/oxide interface, similar to the growth of voids on the β-NiAl phase/oxide interface. However, as already mentioned, the β-phase converts to the γ-phase at the initial stage of the oxidation process, and subsequently, oxide grows from the γ-phase only.

As discussed in Section 4.1, we already know that alumina has a much higher thickness compared to chromia (see Fig. 7). Additionally, $NiAl_2O_4$ spinel grows on the top layer by reacting NiO (which grows at the oxide/air interface) with the initial growth of Al_2O_3 on the β-phase before converting to the γ-phase. Even the growth of $Ni(Al,Cr)_2O_4$ spinel is also reported to grow by the reaction of NiO, Cr_2O_3 and Al_2O_3. Al consumption is higher than Ni and Cr for the growth of thick α-Al_2O_3 oxide layer and mixed oxides. This leads to a higher diffusion flux of Al towards the substrate/oxide interface and the diffusion of Ni and Cr in the opposite direction. Since the diffusion rate of Al is higher in this γ-solid solution phase compared to Cr and Ni [70,71], vacancies are expected to flow away from the interface. Therefore, the void size would be very small (if indeed grown at the early stage of oxidation from the β-phase before converting to the γ-phase), which could not be located and may have little influence. The role of Kirkendall voids is therefore ruled out in the NiCrAlY/oxide system since the oxide layer grows from the γ solid solution phase only after the very initial stage of oxidation with the transformation of β to γ by the loss of Al.

An interdiffusion analysis in the γ-Ni(Pt,Al) solid solution indicates

the reduction in overall interdiffusion coefficients [82]. However, the relative (difference in) mobilities of the elements are expected to be similar in this Ni-rich solid solution phase [73,74,93,94]. Such a characteristic diffusion rate of elements was found in the Ni-rich NiCoFeCrAl solid solution. The relative mobilities of the elements in pure Ni are found to be similar to the binary Ni-Co, ternary Ni-Co-Cr, quaternary Ni-Co-Fe-Cr and quinary Ni-Co-Fe-Cr-Al solid solution phases although interdiffusion coefficients (which are kind of average of diffusion rates of elements) vary differently [71].

Overall, the growth kinetics of the oxide layer on (γ+β)-Ni(Pt)CrAlY is higher compared to β-Ni(Pt)Al because of the growth of non-protective oxides (Cr_2O_3 and spinel). As shown in Fig. 5 and S2(b), the oxide layer thickness on (γ+β)-Ni(Pt)CrAlY after 500 h oxidation is higher than the oxide layer thickness of β-Ni(Pt)Al after 1000 h oxidation at the same temperature of 1100 °C. The addition of Pt does not influence the oxide layer's growth kinetics in both coating alloys. As reported in this study, a comparatively better spallation resistance of the oxide layer is found on β-NiAl [17] compared to (γ+β) NiCrAlY. The main reason for the spallation of oxide on β-NiAl is reported to be the growth of Kirkendall voids at the substrate oxide interface. Since these voids do not grow at the (γ+β) NiCrAlY/oxide interface, the failure could be due to other non-protective oxides. The volume change associated with the transformation of NiO, Cr_2O_3, and Al_2O_3 to spinel may have adverse effects, including the evaporation of Cr as CrO_3 leading to a porous structure [50]. It is also possible that the increase in strain energy with the growth oxide layer on Ni(Pt)CrAlY is also higher because of the additional growth of non-protective oxides with a higher rate compared to the growth of only α-Al_2O_3 on β-Ni(Pt)Al with a much slower growth rate. The addition of Pt improved spallation resistance for both types of coating alloys. The major reason for improving spallation resistance of β-Ni(Pt)Al is believed to be because of the suppression of Kirkendall voids. However, since Pt addition improved spallation resistance for (γ+β) Ni(Pt)CrAlY bond coat alloys as well in the absence of Kirkendall voids, the possibility of improving adhesive strength between substrate and oxide cannot be ruled out.

To compare the growth of the interdiffusion zone between CMSX-4 superalloy and two types of bond coats (i.e. β-Ni(Pt)Al and (γ+β) Ni(Pt)CrAlY), we need to discuss the growth of the interdiffusion zone between β-NiAl bond coat alloy and CMSX-4 alloy first. The growth of the interdiffusion zone between the superalloy and two bond coat alloys, i.e. β-NiAl and β-Ni(10Pt)Al, are shown in Fig. 19. The interdiffusion zone grows with two distinct sublayers: precipitate containing interdiffusion zone i.e. grown from the superalloy and precipitate free sublayer i.e. grown from the bond coat. The Kirkendall marker plane demarcates these two sublayers, indicating the growth from different substrates differently. The precipitate containing the interdiffusion zone can be seen in the BSE micrograph. The thickness of the precipitate-free interdiffusion zone can be understood from the composition profile. The growth sequence of the phase layers in the precipitate-containing interdiffusion zone can be better understood from Fig. 19(a). It highlights the growth of the phases in the sublayer that is grown from the superalloy. The (γ+γ') superalloy first converts to (γ+γ'+β) phases with the loss of Ni from the Ni-rich superalloy and the addition of Al that is diffused from the relatively Al-rich bond coat. The solubility limits of various refractory elements are relatively low in γ' and even lower in the β-phase. Therefore, these elements grow as precipitates with this phase conversion [19,21]. Following, the (γ'+β) phase mixture grows along with precipitates. Next, only the β-phase with a fraction of precipitates grows in the interdiffusion zone. On the other side of the Kirkendall marker plane, the precipitate-free interdiffusion zone grows with the loss of Al from the bond coat and the addition of other elements that diffuse from the superalloy. The thickness of the precipitate-free interdiffusion zone is much higher because of the presence of high melting point refractory elements with very low concentration and in the absence of precipitates through which the diffusion rates of elements are expected to be very low. As shown in Fig. 19(b), the growth mechanism of the phases remains similar when Pt is added to the bond coat. However, there is an increase in interdiffusion zone length for both sublayers. The increase is very significant for the precipitate-free sublayer grown from the bond coat.

A few important characteristics should be noted for the comparison of the interdiffusion zone between two types of bond coat alloys (β-NiAl and (β+γ)-NiCrAlY) and the superalloy. Both Ni and Al go through regular downhill diffusion in β-Ni(Pt)Al/CMX4 systems such that Ni diffuses from a relatively Ni-rich superalloy towards a Ni-lean bond coat. The diffusion direction of Al is opposite, i.e. from a relatively Al-rich bond coat to an Al-lean superalloy. Therefore, the thickness of the total interdiffusion zone thickness is higher for β-NiAl coating alloy compared to (γ+β) NiCrAlY, in which Al goes through uphill diffusion when coupled with CMSX-4 superalloy. It should be noted here that the interdiffusion zone between superalloy and (γ+β) NiCrAlY is grown for 64 h, and superalloy and β-NiAl is grown for 100 h. For diffusion-

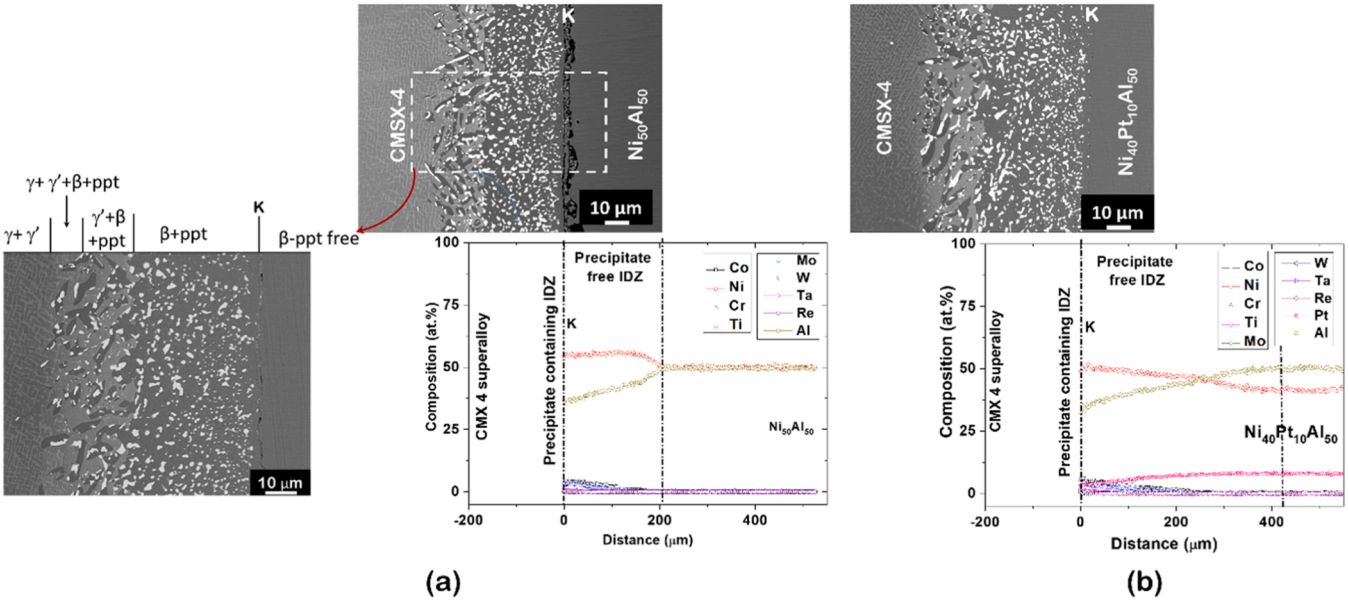

Fig. 19. Interdiffusion zone between CMX4 superalloy between (a) β-Ni50Al, and (b) β-Ni(10Pt)50Al annealed at 1100 °C for 100 h [17].

controlled growth, we consider the square of the thickness interdiffusion zone proportional to the annealing time. Therefore, taking 8/10, i.e. 0.8 times the interdiffusion zone thickness of β-NiAl/CMSX4 superalloy, can be compared with the interdiffusion zone thickness between NiCrAlY/CMSX superalloy. Another reason for the higher thickness of the interdiffusion zone is the growth of the β-phase with higher diffusivity of elements for β-NiAl coating compared to γ and γ' phases, which are grown for (γ+β) NiCrAlY. The interdiffusion rates of elements are higher in the β-phase [21,83] compared to the γ and γ' phases [94,95] because of the presence of constitutional defects (vacancies and antisites) with very high concentrations. Therefore, a major part of the interdiffusion zone is covered by the β-phase for β-NiAl based coatings. Since the solubility of high melting point refractory elements such as W, Re, Ta, etc. has much lower solubility in the β-phase compared to γ and γ' phases, the fraction of the deleterious precipitates is also higher for β-NiAl coating alloy. On the otherhand, Jackson and Raiden have shown that a relatively thick platinum layer of 25 μm restricts the the initial reaction-diffusion during, which reduces the refractory metal elements loss from the substrate and thereby smaller content in the outer regions of the coating. However, a thiner Pt layer did not show this beneficial role [96]. Pt addition to (γ+β) NiCrAlY reduced the interdiffusion zone thickness and growth of precipitates because of decreased diffusion coefficients in the γ and γ' phases and increased the uphill diffusion of Al. This led to a reduction in unwanted loss of Al in the interdiffusion zone. However, adding Pt to β-NiAl increased the interdiffusion zone thickness by increasing the diffusion rate of elements in the β-phase, leading to an increase in the unwanted loss of Al. A diffusion analysis in β-NiAl indicates the increase in defect concentrations (vacancies and antisites) and decreased migration energy because of Pt addition, which mediates the diffusion process [21].

It is already known that the spallation resistance of oxide on β-NiAl is better because of the growth of only α-Al_2O_3 than (γ+β) NiCrAlY because of the growth of other non-protective oxides along with α-Al_2O_3. Pt addition improved spallation resistance for both types of coating alloys. Vande Put et al. discussed the role of peroxidation on spallation resistance before deposition of ceramic top coat enhanced spallation resistance [97]. Al loss in the interdiffusion zone and growth of deleterious phases act in opposite ways because of Pt addition in the NiCrAlY coating compared to β-NiAl coating. Pt addition to β-NiAl increases the Al diffusion rate, leading to a higher loss of Al from the bond coat alloy and, therefore, the growth of a higher fraction of TCP phases in the interdiffusion zone. In contrast, Pt addition to (β+γ) NiCrAlY reduces the loss of Al by increasing the uphill diffusion and, therefore, the growth of a lower fraction of TCP phases.

5. Conclusions

The beneficial role of the addition of Pt in β-NiAl diffusion coating by improving the spallation resistance of the oxide layer (α-Al_2O_3) by reducing the sulphur segregation is well known [41,42]. This has significantly improved thermal cycle resistance even in the air without sulphur resources [17]. However, Pt addition has a deleterious effect on the growth of brittle precipitate-containing interdiffusion zone, which increases significantly because of the increase in defects assisting the diffusion process. In this study, we have shown the beneficial role of Pt addition in NiCrAlY on spallation resistance and in reducing the precipitate-containing interdiffusion zone. The experiments were conducted at 1100 °C for easy analysis through accelerated growth of the oxide layer and interdiffusion zone in the laboratory. The outcome of this study can be summarized as:

- The addition of Pt does not change the relative volume fraction of γ and β significantly in the (γ+β) NiCrAlY. However, Pt is found to partition with higher content in β than the γ phase. Y is found as a Ni_5Y compound at the γ/β phase.
- At the initial stage, the surface morphological characteristics differ depending on the oxidation of the γ- or the β-phase. With the loss of Al, the β-phase converts to the γ-phase, and the subsequent oxidation process continues based on the compositional distribution of this phase during oxidation.
- Other than the continuous layers of α-Al_2O_3 and Cr_2O_3, a few products of oxides are also found to grow, such as $YAlO_3$, $NiCr_2O_4$ and $NiAl_2O_4$. The overall growth rate of the oxide phases in Ni(Pt)CrAlY is found to be higher compared to the growth rate of the only oxide phase α-Al_2O_3 on another type of bond coat β-Ni(Pt)Al since the diffusion rates of elements are known to be very low through α-Al_2O_3 compared to the other oxides.
- The spallation resistance of the oxide layer upon cooling to room temperature after isothermal annealing increases significantly with the addition of Pt. Adding Y is known to improve spallation resistance to a certain extent. However, the presence of Pt and Y greatly improved the spallation resistance.
- Pt addition to NiCrAlY improves the oxide spallation resistance. Pt addition also reduces the growth of the deleterious precipitate-containing interdiffusion zone. It also reduces the unwanted loss of Al in this zone since the Al content in the bond coat is very important for the service life of the coating layer, providing a continuous supply for the protective oxide layer growth after spallation.
- A comprehensive analysis and explanation are given for the difference in growth characteristics of the interdiffusion zone between superalloy and two types of coating considered in this study.

Author agreement statement

I, on behalf of all authors, declare that this manuscript is original, has not been published previously, and is not currently under consideration for publication elsewhere. I further confirm that all authors have read and approved the final version of the manuscript.

CRediT authorship contribution statement

Ujjval Bansal: Writing – original draft, Methodology, Investigation, Formal analysis, Data curation, Conceptualization. **Neelamegan Esakkiraja:** Writing – review & editing, Methodology, Investigation, Formal analysis, Data curation, Conceptualization. **Tanaji Paul:** Writing – review & editing, Methodology, Investigation, Formal analysis, Data curation, Conceptualization. **Thangaraj Baskaran:** Writing – review & editing, Methodology, Investigation, Formal analysis, Data curation, Conceptualization. **Praveen Kumar:** Supervision. **Raju Ravi:** Supervision. **Aloke Paul:** Writing – review & editing, Visualization, Supervision, Funding acquisition. **Vikram Jayaram:** Writing – review & editing, Supervision.

Declaration of Competing Interest

The authors declare that they have no known competing financial interests or personal relationships that could have appeared to influence the work reported in this paper.

Data availability

Data will be made available on request.

Appendix A. Supporting information

Supplementary data associated with this article can be found in the online version at doi:10.1016/j.corsci.2024.112485.

References

[1] J.T. DeMasi-Marcin, D.K. Gupta, Protective coatings in the gas turbine engine, Surf. Coat. Technol. 68–69 (1994) 1–9.
[2] S.R.J. Saunders, J.R. Nicholls, Coatings and surface treatments for high temperature oxidation resistance, Mater. Sci. Technol. 5 (1989) 780–798.
[3] G.W. Goward, Progress in coatings for gas turbine airfoils, Surf. Coat. Technol. 108– 109 (1998) 73–79.
[4] A.G. Evans, D.R. Mumm, J.W. Hutchinson, G.H. Meier, F.S. Pettit, Mechanisms controlling the durability of thermal barrier coatings, Prog. Mater. Sci. 46 (2001) 505–553.
[5] J.R. Nicholls, Designing oxidation-resistant coatings, JOM 52 (2000) 28–35.
[6] N.P. Padture, M. Gell, E.H. Jordan, Thermal barrier coatings for gas-turbine engine applications, Sci 296 (2002) 280–284.
[7] J. Angenete, K. Stiller, E. Bakchinova, Microstructural and microchemical development of simple and Pt-modified aluminide diffusion coatings during long term oxidation at 1050 °C, Surf. Coat. Technol. 176 (2004) 272–283.
[8] Y. Chen, X. Zhao, P. Xiao, Effect of microstructure on early oxidation of MCrAlY coatings, Acta Mater. 159 (2018) 150–162.
[9] X. Jiang, W. Song, J. Liang, X. Tao, D. Zhang, Y. Zhou, X. Sun, J. Li, Effect of coatings on oxidation behavior of a fourth generation Ni-based single crystal superalloys at ultra high temperature, Surf. Coat. Technol. 479 (2024) 130592.
[10] P.Y. Hou, K.F. McCarty, Surface and interface segregation in β-NiAl with and without Pt addition, Scr. Mater. 54 (2006) 937–941.
[11] L. Rivoaland, V. Maurice, P. Josso, M.-P. Bacos, P. Marcus, The effect of sulfur segregation on the adherence of the thermally-grown oxide on NiAl—II: the oxidation behavior at 900°C of standard, desulfurized or sulfur-doped NiAl(001) single-crystals, Oxid. Met 60 (2003) 159–178.
[12] J.A. Haynes, B.A. Pint, K.L. More, Y. Zhang, I.G. Wright, Influence of sulfur, platinum, and hafnium on the oxidation behavior of CVD NiAl bond coatings, Oxid. Met 58 (2002) 513–544.
[13] D. Poquillon, D. Oquab, B. Viguier, F. Sénocq, D. Monceau, High-temperature oxidation kinetics of NiAl single crystal and oxide spallation as a function of crystallographic orientation, Mater. Sci. Eng. A 381 (2004) 237–248.
[14] H. Svensson, M. Christensen, P. Knutsson, G. Wahnström, K. Stiller, Influence of Pt on the metal–oxide interface during high temperature oxidation of NiAl bulk materials, Corros. Sci. 51 (2009) 539–546.
[15] Y. Cadoret, M.P. Bacos, P. Josso, V. Maurice, P. Marcus, S. Zanna, Effect of Pt additions on the sulfur segregation, void formation and oxide scale growth of cast nickel aluminides, Mater. Sci. Forum 461–464 (2004) 247–254.
[16] R. Molins, I. Rouzou, P. Hou, Chemical and morphological evolution of a (NiPt)Al bondcoat, Oxid. Met. 65 (2006) 263–283.
[17] T. Baskaran, N. Esakkiraja, C. Samartha, P. Kumar, V. Jayaram, A. Paul, Effect of addition of Pt, Pd and Ir to β-NiAl-bond coat on oxidation resistance and growth of interdiffusion zone, Surf. Coat. Technol. 426 (2021) 127766.
[18] Y. Cadoret, D. Monceau, M.-P. Bacos, P. Josso, V. Maurice, P. Marcus, Effect of platinum on the growth rate of the oxide scale formed on cast nickel aluminide intermetallic alloys, Oxid. Met. 64 (2005) 185–205.
[19] P. Kiruthika, S.K. Makineni, C. Srivastava, K. Chattopadhyay, A. Paul, Growth mechanism of the interdiffusion zone between platinum modified bond coats and single crystal superalloys, Acta Mater. 105 (2016) 438–448.
[20] N. Esakkiraja, A. Vishwakarma, S.K. Makineni, V. Jayaram, T. Hickel, S. V. Divinski, A. Paul, Diffusion-controlled growth and microstructural evolution between Pt and Pd containing B2-NiAl bondcoats and Ni-based single crystal superalloy, Acta Mater. 266 (2024) 119687.
[21] N. Esakkiraja, A. Gupta, V. Jayaram, T. Hickel, S.V. Divinski, A. Paul, Diffusion, defects and understanding the growth of a multicomponent interdiffusion zone between Pt-modified B2 NiAl bond coat and single crystal superalloy, Acta Mater. 195 (2020) 35–49.
[22] P. Kiruthika, A. Paul, A pseudo-binary interdiffusion study in the β-Ni(Pt)Al phase, Philos. Mag. Lett. 95 (2015) 138–144.
[23] T. Amano, Y. Takezawa, A. Shiino, T. Shishido, Surface morphology of scale on FeCrAl (Pd, Pt, Y) alloys, J. Alloy Compd. 452 (2008) 16–22.
[24] J.K. Tien, F.S. Pettit, Mechanism of oxide adherence on Fe-25Cr-4Al (Y or Sc) alloys, Metall. Trans. 3 (1972) 1587–1599.
[25] S. Kim, C.-H. Lee, T. Kim, J.H. Jang, J. Moon, D.F. Falaakh, J.H. Kim, C.B. Bahn, Effects of yttrium on the oxidation behavior of Fe13Cr6AlY alloys under 1200 °C steam, J. Alloy Compd. 960 (2023) 170642.
[26] R. Chen, X. Gong, Y. Wang, G. Qin, N. Zhang, Y. Su, H. Ding, J. Guo, H. Fu, Microstructure and oxidation behaviour of plasma-sprayed NiCoCrAlY coatings with and without Ta on Ti44Al6Nb1Cr alloys, Corros. Sci. 136 (2018) 244–254.
[27] J.J. Liang, H. Wei, Y.L. Zhu, X.F. Sun, Z.Q. Hu, M.S. Dargusch, X.D. Yao, Influence of Re on the Properties of a NiCoCrAlY Coating Alloy, J. Mater. Sci. Technol. 27 (2011) 408–414.
[28] N. Czech, F. Schmitz, W. Stamm, Improvement of MCrAlY coatings by addition of rhenium, Surf. Coat. Technol. 68-69 (1994) 17–21.
[29] L. Shi, L. Xin, X. Wang, X. Wang, H. Wei, S. Zhu, F. Wang, Influences of MCrAlY coatings on oxidation resistance of single crystal superalloy DD98M and their inter-diffusion behaviors, J. Alloy Compd. 649 (2015) 515–530.
[30] W. Duan, Y. Li, W. Qiang, Effect of Hf-doped MCrAlY alloy on the structure and properties of thermally grown oxide layer, J. Mater. Eng. Perform. (2023).
[31] W. Duan, B. Huang, Y. Li, X. Huang, M. Zhou, W. Qiang, Hf and Ta co-doping MCrAlY alloy to improve the lifetime of coatings, Surf. Coat. Technol. 468 (2023) 129781.
[32] D. Monceau, D. Oquab, C. Estournes, M. Boidot, S. Selezneff, Y. Thebault, Y. Cadoret, Pt-modified Ni aluminides, MCrAlY-base multilayer coatings and TBC systems fabricated by Spark Plasma Sintering for the protection of Ni-base superalloys, Surf. Coat. Technol. 204 (2009) 771–778.
[33] S.-W. Myoung, S.-H. Park, P.-H. Lee, Y.-G. Jung, D. Joo, K.-H. Lee, H.-S. Lee, U. Paik, Phase transformation and oxidation behavior of Pt-modified MCrAlY coatings, Prog. Org. Coat. 61 (2008) 316–320.
[34] A. Khan, P. Song, T. Huang, Y. Zhou, X. Xiong, C. Li, J. Lü, R. Chen, J. Lu, Diffusion characteristics and structural stability of Pt modified β-NiAl/γ′-Ni3Al within NiCoCrAl alloy at high temperature, Appl. Surf. Sci. 476 (2019) 1096–1107.
[35] R. Cuenca-Álvarez, S.D. de la Torre, F.J. López, Mechanical dispersion of platinum particles and its effect on the microstructure of MCrAlY alloy prepared by SPS, Powder Technol. 291 (2016) 193–200.
[36] D. Blavette, P. Caron, T. Khan, An atom probe investigation of the role of rhenium additions in improving creep resistance of Ni-base superalloys, Scr. Metall. 20 (1986) 1395–1400.
[37] C. Kwakernaak, W.G. Sloof, T.J. Nijdam, Microstructure refinement of NiCoCrAlY alloys by laser surface melting, Metall. Mater. Trans. A 37 (2006) 695–703.
[38] T.J. Nijdam, W.G. Sloof, Effect of Y distribution on the oxidation kinetics of NiCoCrAlY bond coat alloys, Oxid. Met. 69 (2008) 1–12.
[39] T.J. Nijdam, L.P.H. Jeurgens, J.H. Chen, W.G. Sloof, On the Microstructure of the initial oxide grown by controlled annealing and oxidation on a NiCoCrAlY bond coating, Oxid. Met. 64 (2005) 355–377.
[40] K.A. Marino, E.A. Carter, The effect of platinum on defect formation energies in β-NiAl, Acta Mater. 56 (2008) 3502–3510.
[41] K.A. Marino, B. Hinnemann, E.A. Carter, Atomic-scale insight and design principles for turbine engine thermal barrier coatings from theory, Proc. Natl. Acad. Sci. U. S. A. 108 (2011) 5480–5487.
[42] M.W. Brumm, H.J. Grabke, The oxidation behaviour of NiAl-I. Phase transformations in the alumina scale during oxidation of NiAl and NiAl-Cr alloys, Corros. Sci. 33 (1992) 1677–1690.
[43] J.K. Doychak, The Evolution and Growth of Al2O3 Scales on β-NiAl, Department of Metallurgy and Materials Science, Case Western Reserve University, 1986.
[44] T.J. Nijdam, L.P.H. Jeurgens, W.G. Sloof, Modelling the thermal oxidation of ternary alloys—compositional changes in the alloy and the development of oxide phases, Acta Mater. 51 (2003) 5295–5307.
[45] S.W. Guan, Oxygen solubility and a criterion for the transition from internal to external oxidation of ternary alloys, Oxid. Met. 42 (1994) 375–391.
[46] A. Paul, T. Laurila, V. Vuorinen, S.V. Divinski, Thermodynamics, Diffusion and the Kirkendall Effect in Solids, Springer International Publishing, Cham, 2014.
[47] V.K. Tolpygo, D.R. Clarke, Microstructural evidence for counter-diffusion of aluminum and oxygen during the growth of alumina scales, Mater. High. Temp. 20 (2003) 261–271.
[48] C. Jiang, L. Qian, M. Feng, H. Liu, Z. Bao, M. Chen, S. Zhu, F. Wang, Benefits of Zr addition to oxidation resistance of a single-phase (Ni,Pt)Al coating at 1373 K, J. Mater. Sci. Technol. 35 (2019) 1334–1344.
[49] V.K. Tolpygo, D.R. Clarke, Microstructural study of the theta-alpha transformation in alumina scales formed on nickel-aluminides, Mater. High. Temp. 17 (2000) 59–70.
[50] F. Ghadami, A. Sabour Rouh Aghdam, S. Ghadami, A comprehensive study on the microstructure evolution and oxidation resistance of conventional and nanocrystalline MCrAlY coatings, Sci. Rep. 11 (2021) 875.
[51] A. Rabiei, Failure mechanisms associated with the thermally grown oxide in plasma-sprayed thermal barrier coatings, Acta Mater. 48 (2000) 3963–3976.
[52] L. Ajdelsztajn, J.A. Picas, G.E. Kim, F.L. Bastian, J. Schoenung, V. Provenzano, Oxidation behavior of HVOF sprayed nanocrystalline NiCrAlY powder, Mater. Sci. Eng. A 338 (2002) 33–43.
[53] W.R. Chen, X. Wu, D. Dudzinski, P.C. Patnaik, Modification of oxide layer in plasma-sprayed thermal barrier coatings, Surf. Coat. Technol. 200 (2006) 5863–5868.
[54] A. Feizabadi, M. Salehi Doolabi, S.K. Sadrnezhaad, M. Rezaei, Cyclic oxidation characteristics of HVOF thermal-sprayed NiCoCrAlY and CoNiCrAlY coatings at 1000 °C, J. Alloy Compd. 746 (2018) 509–519.
[55] J.G. Smeggil, A.J. Shuskus, The oxidation behavior of CoCrAlY, CoCrAl and yttrium-implanted CoCrAl alloys compared and contrasted, Surf. Coat. Technol. 32 (1987) 57–68.
[56] D. Migas, B. Chmiela, H. Myalska-Głowacka, G. Moskal, K. Matus, R. Swadźba, The effect of yttrium on oxide scale growth on Co-Al-W-based superalloys, Corros. Sci. 208 (2022) 110674.
[57] E.A.G. Shillington, D.R. Clarke, Spalling failure of a thermal barrier coating associated with aluminum depletion in the bond-coat, Acta Mater. 47 (1999) 1297–1305.
[58] J. Allen Haynes, E. Douglas Rigney, M.K. Ferber, W.D. Porter, Oxidation and degradation of a plasma-sprayed thermal barrier coating system, Surf. Coat. Technol. 86– 87 (1996) 102–108.
[59] C.H. Lee, H.K. Kim, H.S. Choi, H.S. Ahn, Phase transformation and bond coat oxidation behavior of plasma-sprayed zirconia thermal barrier coating, Surf. Coat. Technol. 124 (2000) 1–12.
[60] W.R. Chen, X. Wu, B.R. Marple, P.C. Patnaik, Oxidation and crack nucleation/growth in an air-plasma-sprayed thermal barrier coating with NiCrAlY bond coat, Surf. Coat. Technol. 197 (2005) 109–115.
[61] R. Mévrel, State of the art on high-temperature corrosion-resistant coatings, Mater. Sci. Eng. A 120– 121 (1989) 13–24.
[62] W.G. Sloof, T.J. Nijdam, On the high-temperature oxidation of MCrAlY coatings, Int. J. Mater. Res 100 (2009) 1318–1330.
[63] C.G. Levi, E. Sommer, S.G. Terry, A. Catanoiu, M. Rühle, Alumina grown during deposition of thermal barrier coatings on NiCrAlY, J. Am. Ceram. Soc. 86 (2003) 676–685.

[64] T.J. Nijdam, C. Kwakernaak, W.G. Sloof, The effects of alloy microstructure refinement on the short-term thermal oxidation of NiCoCrAlY alloys, Metall. Mater. Trans. A 37 (2006) 683–693.
[65] T.J. Nijdam, L.P.H. Jeurgens, W.G. Sloof, Promoting exclusive α-Al2O3 growth upon high-temperature oxidation of NiCrAl alloys: experiment versus model predictions, Acta Mater. 53 (2005) 1643–1653.
[66] R.S. Roth, Phase equilibria diagrams. Phase Diagrams for Ceramists, American Ceramic Society, 1995.
[67] J.S. Kirkaldy, Diffusion in multicomponent metallic systems iii — the motion of planar phase interfaces, Can. J. Phys. 36 (1958) 917–925.
[68] J.S. Kirkaldy, L.C. Brown, Diffusion behaviour in ternary, multiphase systems, Can. Metall. Q. 2 (1963) 89–115.
[69] J.B. Clarke, Conventions for plotting the diffusion paths in multiphase ternary diffusion couples on the isothermal section of a ternary phase diagram, Trans. Met. Soc. AIME 227 (1963) 1250–1251.
[70] J.A. Nesbitt, R.W. Heckel, Interdiffusion in Ni-Rich, Ni-Cr-Al alloys at 1100 and 1200 °C: Part I. Diffusion paths and microstructures, Metall, Trans. A 18 (1987) 2061–2073.
[71] A. Dash, S. Bhattacharyya, A. Paul, Estimation of diffusion coefficients in NiCoFeCrAl multi-principal element alloy following an inventive design strategy of diffusion couples, Acta Mater. 260 (2023) 119296.
[72] V.K. Tolpygo, J.R. Dryden, D.R. Clarke, Determination of the growth stress and strain in α-Al2O3 scales during the oxidation of Fe–22Cr–4.8Al–0.3Y alloy, Acta Mater. 46 (1998) 927–937.
[73] M.S.A. Karunaratne, R.C. Reed, Interdiffusion of the platinum-group metals in nickel at elevated temperatures, Acta Mater. 51 (2003) 2905–2919.
[74] A. Janotti, M. Krčmar, C.L. Fu, R.C. Reed, Solute diffusion in metals: larger atoms can move faster, Phys. Rev. Lett. 92 (2004) 085901.
[75] A. Paul, V. Divinski. Diffusion analysis in material applications, Elsevier, Amsterdam, 2017.
[76] J.S. Kirkaldy, G.R. Purdy, Diffusion in multicomponent metallic systems. X. Diffusion at and near ternary critical states, Can. J. Phys. 47 (1969) 865–871.
[77] J.S. Kirkaldy, D.J. Young, Diffusion in the condensed state. Institute of Metals; Institute of Metals, Brookfield, VT, USA, North America, London, 1987.
[78] N. Dupin, B. Sundman, A thermodynamic database for Ni-base superalloys, Scand. J. Metall. 30 (2001) 184–192.
[79] J.-O. Andersson, T. Helander, L. Höglund, P. Shi, B. Sundman, Thermo-Calc & DICTRA, computational tools for materials science, Calphad 26 (2002) 273–312.
[80] Thermo-Calc Software, (n.d.). ⟨https://thermocalc.com/products/databases/nickel-based-alloys/⟩.
[81] A. Paul, S.V. Divinski (Eds.), Diffusion fundamentals and techniques, Elsevier, Amsterdam, 2017.
[82] S. Hayashi, D.J. Sordelet, L.R. Walker, B. Gleeson, Interdiffusion in Pt-Containing γ-Ni and γ′-Ni3Al Alloys at 1150°C, Mater. Trans. 49 (2008) 1550–1557.
[83] A. Paul, A.A. Kodentsov, F.J.J.Van Loo, On diffusion in the β-NiAl phase, J. Alloy Compd. 403 (2005) 147–153.
[84] A. Paul, A.A. Kodentsov, F.J.J. Van Loo, Bifurcation of the Kirkendall plane during interdiffusion in the intermetallic compound β-NiAl, Acta Mater. 52 (2004) 4041–4048.
[85] M.W. Brumm, H.J. Grabke, Oxidation behaviour of NiAl—II. Cavity formation beneath the oxide scale on NiAl of different stoichiometries, Corros. Sci. 34 (1993) 547–561.
[86] E.J. Felten, F.S. Pettit, Development, growth, and adhesion of Al2O3 on platinum-aluminum alloys, Oxid. Met. 10 (1976) 189–223.
[87] E.J. Felten, Use of platinum and rhodium to improve oxide adherence on Ni-8Cr-6Al alloys, Oxid. Met. 10 (1976) 23–28.
[88] R. Bouchet, R. Mevrel, Calculating the composition-dependent diffusivity matrix along a diffusion path in ternary systems, Calphad 27 (2003) 295–303.
[89] B. Gleeson, W. Wang, S. Hayashi, D.J. Sordelet, Effects of platinum on the interdiffusion and oxidation behavior of Ni-Al-based alloys, Mater. Sci. Forum 461–464 (2004) 213–222.
[90] S. Hayashi, W. Wang, D.J. Sordelet, B. Gleeson, Interdiffusion behavior of Pt-modified γ-Ni + γ′-Ni3Al alloys coupled to Ni-Al-based alloys, Metall. Mater. Trans. A 36 (2005) 1769–1775.
[91] E. Copland, Partial thermodynamic properties of γ′-(Ni,Pt)3Al in the Ni-Al-Pt system, J. Phs. Eqil. Diff 28 (2007) 38–48.
[92] G.C. Hou, H. Wei, N.R. Zhao, X.F. Sun, H.R. Guan, Z.Q. Hu, Interdiffusion in the β phase region of the Ni–Al–Cr system, Scr. Mater. 58 (2008) 57–60.
[93] G. Neumann, C. Tuijn. Self-diffusion and impurity diffusion in pure metals: handbook of experimental data, 1. ed, Elsevier, Amsterdam Heidelberg, 2009.
[94] T. Yamamoto, T. Takashima, K. Nishida, Interdiffusion in the ζ-solid solution of a Ni–Al system, J. Jpn. Inst. Met. Mater. 44 (1980) 294–299.
[95] C. Cserháti, A. Paul, A.A. Kodentsov, M.J.H. Van Dal, F.J.J.Van Loo, Intrinsic diffusion in Ni3Al system, Intermetallics 11 (2003) 291–297.
[96] M.R. Jackson, J.R. Rairden, The aluminization of platinum and platinum coated IN 738, Metall. Trans. A 8 (1977) 1697–1707.
[97] A.V. Vande Put, D. Oquab, E. Péré, A. Raffaitin, D. Monceau, Beneficial effect of Pt and Pre-oxidation on the oxidation behaviour of an NiCoCrAlYTa bond coating for thermal barrier coating systems, Oxid. Met. 75 (2011) 247–279.